Université de Montréal

Calibration of the Sensitivity of Perfluorocarbon Mixtures to Nuclear Recoil

par

Jeremy Savoie

Département de physique
Faculté des arts et des sciences

Mémoire présenté en vue de l'obtention du grade de
Maître ès sciences (M.Sc.)
en Physique

31 août 2022

Université de Montréal

Faculté des arts et des sciences

Ce mémoire intitulé

Calibration of the Sensitivity of Perfluorocarbon Mixtures to Nuclear Recoil

présenté par

Jeremy Savoie

a été évalué par un jury composé des personnes suivantes :

Jean-François Arguin
(président-rapporteur)

Alan Robinson
(directeur de recherche)

David Lafrenière
(membre du jury)

Résumé

L'expérience PICO fait partie des chefs de file mondiaux dans la tentative de détection directe de la matière sombre. Cette expérience se spécialise dans l'utilisation des détecteurs à liquide surchauffé pour y parvenir. Le futur détecteur de la collaboration, PICO-500, tentera de détecter les WIMPs (Weakly Interacting Massive Particle) une fois construit dans le laboratoire sous-terrain SNOLAB. Ce détecteur utilisera un mélange de perfluorocarbone comme fluide actif, une nouveauté pour les chambres à bulles. L'utilisation d'un mélange présente des avantages importants dans la conception du détecteur. Celle-ci permettra de diminuer les contraintes d'ingénierie tout en offrant une sensibilité de détection importante.

La chambre à bulles PICO-0.1 est utilisée principalement pour la calibration de perfluorocarbone. À l'aide du tandem situé à l'Université de Montréal et d'une cible de vanadium-51, j'ai pu envoyer des neutrons monoénergétiques afin d'évaluer l'énergie de seuil de la formation de bulles dans ce mélange. Le modèle de Seitz décrivant la formation des bulles a été bien étudié dans le cadre de fluide pur, mais pas dans le cas de mélange de perfluorocarbone. Ce type de calibration effectuée avec le détecteur PICO-0.1 nous a permis de confirmer la validité du modèle de Seitz et que les effets du transport de masse peut être négligés pour ce mélange. La vérification de cette hypothèse était cruciale à la compréhension de la dynamique impliquée dans la formation des bulles et nécessaire pour l'utilisation du futur détecteur PICO-500.

Mots-clés : matière sombre, WIMP, PICO, chambre à bulles, modèle de Seitz, mélange de perfluorocarbone, recul nucléaire

Abstract

The PICO experiment is one of the world's leading experiments in the effort to directly detect dark matter. This experiment specializes in the use of superheated liquid detectors for that end. The future PICO detector, PICO-500, will attempt to detect WIMPs (Weakly Interacting Massive Particle) once it will be built at the underground laboratory SNOLAB. This detector will use a mixture of perfluorocarbon as an active fluid, a novelty for bubble chambers in dark matter searches. The use of mixture presents important advantages in the design of this detector. This will allow to lessen some of the engineering constraints while still offering a high sensitivity.

The PICO-0.1 bubble chamber is mainly used for the calibration of perfluorocarbon. With the help of the Université de Montréal's tandem and a target of vanadium-51, I was able to send monoenergetic neutrons to evaluate the threshold energy of bubble nucleation of this mixture. The Seitz model describing bubble formation has been widely studied in the context of pure fluid, but not in the case of perfluorocarbon mixture. This type of calibration with PICO-0.1 has allowed us to confirm that the Seitz model still apply and that the effects of mass transport can be neglected for this mixture. The verification of this hypothesis was crucial to the understanding of the dynamics implicated in bubble formation and was necessary for the future use of PICO-500.

Keywords: dark matter, WIMP, PICO, bubble chamber, Seitz model, perfluorocarbon mixture, nuclear recoil

Contents

List of Tables

List of Figures

Liste des sigles et des abréviations

WIMP	Particule massive intéragissant faiblement, de l'anglais *Weakly interacting massive particle*
SUSY	Supersymétrie, de l'anglais *Supersymmetry*
LAB	Alkyl benzène linéaire , de l'anglais *Linear alkyl benzene*
DAQ	Système d'acquisition de données, de l'anglais *Data Acquisition System*
SCA	Analyseur monocanal, de l'anglais *Single-channel analyzer*
RTD	Détecteur thermique de résistance, de l'anglais *Resistance temperature detector*

Acknowledgements

Firstly, I would like to thank Alan Robinson for his guidance, his patience and for sharing his passion of particle physics. It is not always easy to value your own work amongst the entirety of a collaboration, but you have reassured me that this work was needed. Many of my friends or colleagues quit academics after a bad experience. I want to thank you for giving me a very good experience and for giving me opportunities that will help me in my future.

I would like to thank the students of our group: David, Émile, François, Gabriel, Hantz, Noah, Shiva and Valérie for your help, for listening, for your suggestions and for the good times that we shared at the bunker. It wasn't easy working alone at the lab during the pandemic and our time together really shone some light through those thick concrete walls.

I would like to the thank the many people at the bunker whose help was invaluable: Fabrice, Martin, Mathieu, Nick and Viktor. Their expertise and their willingness to help me is extremely appreciated and I cannot thank you enough for the time that you spent helping me during the many weeks of data acquisition.

I want to thank my family for the endless support. It wasn't always easy being away and working without end on so many different projects, but you've always been there and gave me your support. I promise to come visit more often.

I would like to thank my girlfriend Érika for supporting me during all this time, for listening to me complain and for being there when I was too tired to do anything. I can't thank you enough for what you have done for me.

I would like to thank my friends: Amélie, Francis, Gabriel, Gonzo, Hermann, Jacques, Karina, Loic, Maxime, Moni, Pierre, Rezan and Sidric. I couldn't have completed this without all of the good times that we spent together. It gave me the energy and the determination needed to complete it.

I would also like to thank Jean-François for his support and for your counsel. I really appreciate the time that you took to give me advise even though I'm not one of your students. I also appreciate the value that you give to my suggestions and opinions.

Preface - Effects of Mental Health on Learning and Productivity

This preface will help to contextualize the situation in which the research in this memoir, and more broadly how every research student in Quebec universities, takes place. Understanding the effects of mental health on learning and productivity can help department/faculty to improve the work environment and the quality of their programs. This in turn can lead to a better reputation, improve the research output and increase recruit. This preface will give a broad overview of some literature concerning mental well-being of university students.

The World Health Organization defines health as "a state of complete physical, mental and social well-being and not merely the absence of disease or infirmity". Mental health is an important part of our health and poor mental well-being have a lot of impact on our lives. In 2011, MacKean released her report [1] on mental health and well-being of post-secondary students and it showed a stronger prevalence of mental health problems among those students than the rest of the population. In this preface, we will take a look at various studies on post-secondary students' mental well-being to have a better understanding of the current situation, see the impact that mental health can have on different aspects of society and research and what are the various factors that can affect mental well-being.

0.1. Studies on post-secondary mental health

In this section, we will look at the problematic through various mental health studies that looked specifically at mental well-being for post-secondary students. This overview will help us have a general understanding of the current situation. The results of these studies will be compared to see similarity and differences with the general population.

0.1.1. "Ça va?"

In 2016, The Federation of students' association on the University of Montreal Campus (Faécum) made a study called "Ça va?" on the mental well-being of its members. More than

10 000 students both undergraduate and graduate responded to the survey, amounting to nearly a quarter of the students at the University of Montreal (UdeM) at the time. This study looked at 4 different aspects of mental health: depression symptoms, psychological distress, burnout, and suicidal thoughts.

Depression

Depression is defined by the American Psychological Association (APA) dictionary as "a negative affective state, ranging from unhappiness and discontent to an extreme feeling of sadness, pessimism, and despondency that interferes with daily life." In the Faécum study, they measured the symptoms of depression with a PHQ-9 test [2]. This test measures the intensity of the symptoms attributed to depression. The table 0.1 shows the score obtained, the severity associated with that score and the action proposed to treat the symptoms.

Score	Severity measured	Proposed action (when used as a personalized testing)
1 to 4	None	None.
5 to 9	Light	Administer the test again at the next visit.
10 to 14	Moderate	Discuss possible treatments with the patient in case the symptoms worsen.
15 to 19	Moderately severe	Begin a treatment through psychotherapy or pharmaceutical immediately.
20 to 27	Severe	Begin a treatment through psychotherapy or pharmaceutical immediately and if judged too severe, refer to a multidisciplinary team.

Table 0.1. Table categorizing the score of testing on the PHQ-9 [translated from French, 3, tab. 2].

In Figure 0.1, we can see the proportion of people according to their level of symptoms and their level of study (undergraduate, master degree, doctoral study and medical residency). Twenty-two percent of students present symptoms that are high enough to warrant an immediate treatment through either psychotherapy or pharmaceutics. We can observe that depression symptoms seem to affect undergraduate students to a higher level than other students with a percentage of 24.6% of them having a score moderately severe to severe.

Psychological Distress

Psychological Distress is described by the APA dictionary as "a set of painful mental and physical symptoms that are associated with normal fluctuations of mood in most people".

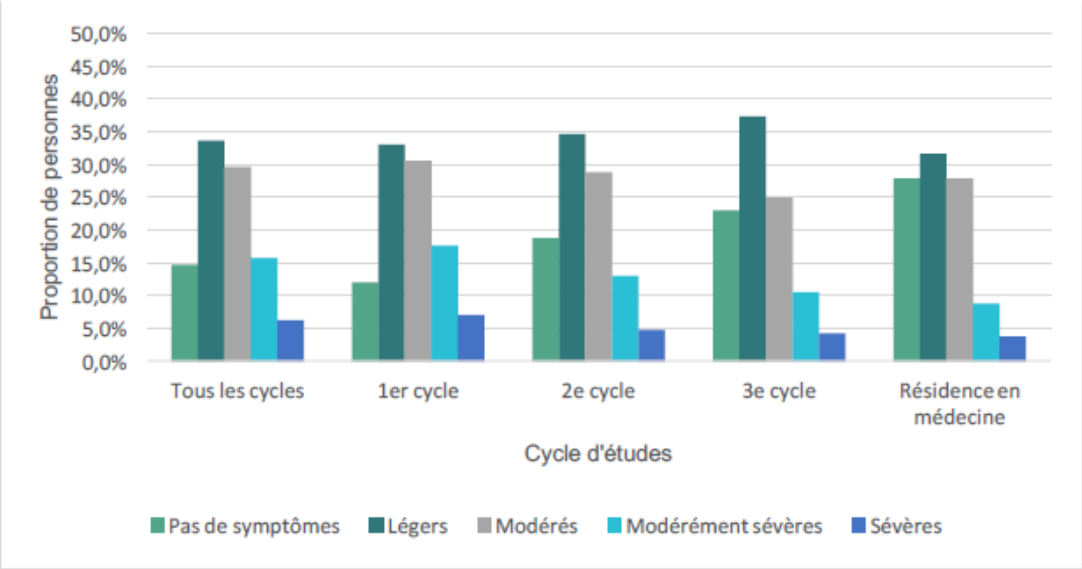

Figure 0.1. Percentage of people presenting symptoms of depression according to their level of study (all cycle, undergraduate, master degree, doctoral study and medical residency). The lighter green is no symptoms, darker green is light symptoms, gray is moderate symptoms, cyan is moderately severe and blue is severe symptoms [translated from French, 3, fig. 1].

Figure 0.2 shows the score on the K6 quiz [4] measuring the psychological distress. The K6, contrary to the PHQ-9, is not a measurement of the intensity of a symptom, but of the total number of different symptoms. 20% of the general population has a score of 7 or higher. For the students, 64% achieved a score that high. This demonstrates that students present significantly more symptoms of psychological distress than the general population.

Burnout

Burnout is defined in the APA dictionary as "a physical, emotional, or mental exhaustion accompanied by decreased motivation, lowered performance, and negative attitudes toward oneself and others." The study measured the symptoms of burnout with a scale called the Maslach Burnout Inventory [5]. In this scale, a person is considered to have symptoms of burnout if they have a high score on three sub-scales: emotional exhaustion, depersonalization and feeling of lack of accomplishment. We can also have an idea of the number of students that are more inclined to experience a burnout by looking for the ones with a high score on two sub-scales. No study was found to have used this scale on the general population of Quebec. Therefore, it would not be adequate to compare the burnout scores of students to the general population since no similar test was conducted on both.

The results showed that about 3.4% of students had a high score on all 3 sub-scale and another 5.8% had a high score on 2 sub-scales. The study also showed that it affected primarily undergraduates with more than 10% having a high score on at least 2 sub-scales

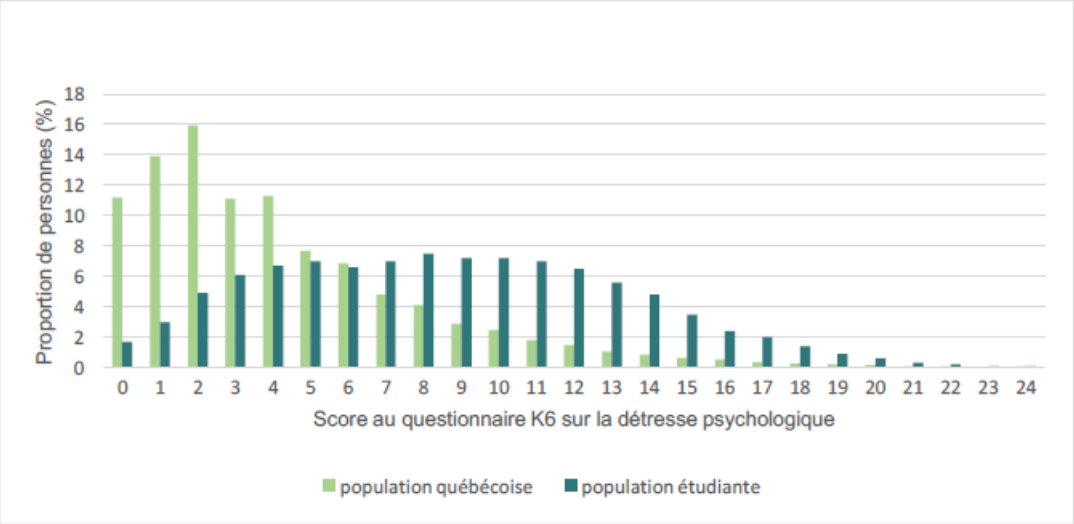

Figure 0.2. Percentage of people with each score on the K6 measuring psychological distress. In light green is the general population and in darker green is the student population [translated from French, 3, fig. 2].

(see Figure 0.3), indicating that they either can be categorized as having a burnout or at risk of developing one. In a later section, we will discuss about various studies measuring the impact of overwork and burnout.

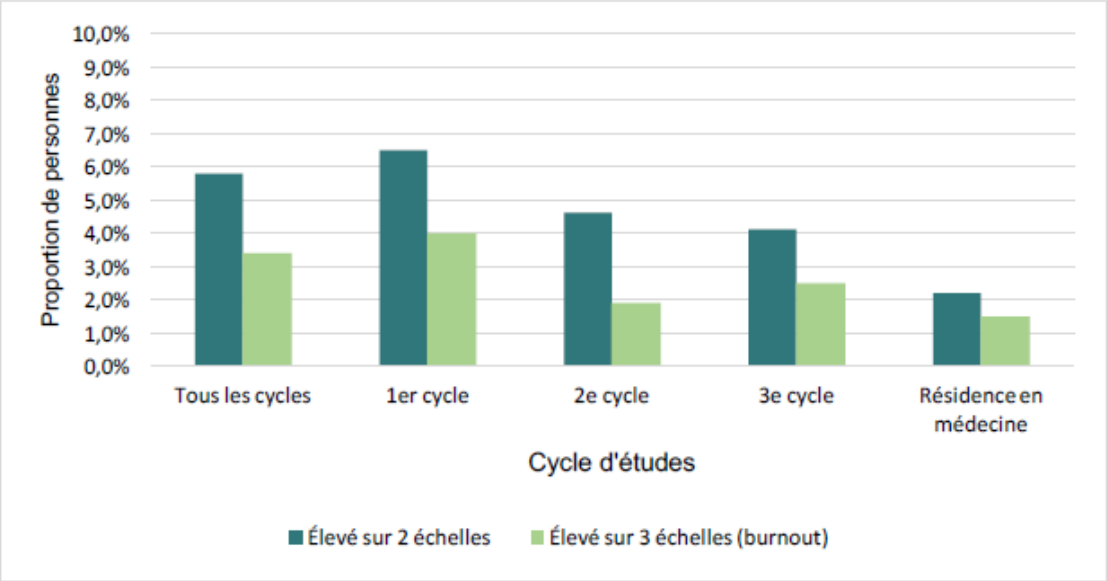

Figure 0.3. Percentage of people with each score on the Maslach, Jackson and Leiter [5]. In light green is a high score on 2 sub-scales and in darker green is a high score on all three sub-scales [translated from French, 3, fig. 3].

Suicidal Ideation

Suicidal ideation is described by the APA dictionary as "thoughts about or a preoccupation with killing oneself, often as a symptom of a major depressive episode." It is an extremely worrisome issue. In Quebec, it is the leading cause of death for people aged less than 35 [6]. It is especially worrisome since some universities often lack the data to indicate how problematic the situation currently is [7]. In 2019, University of Ottawa experienced a mental health crisis with the suicide of 5 students in the span of 10 months [8], and this just prior to the COVID-19 pandemic. This issue launched a series of reports assessing the current mental state of students.

In the "Ça va?" study, they looked whether a person had suicidal thoughts in the past 12 months to measure mainly the situation when the person was at the university. They measured it with two questions, one for having serious suicidal thoughts and another about failed suicide attempts. For all cycle, 7.8% of the students reported having seriously thought of ending their lives and 1.2% had attempted to commit suicide in the past 12 months. In comparison, only 2.6% of the general population of the same age reported having seriously thought about ending their life and 0.6% having attempted to end it [3]. We can remark that the student population is more at risk of suicidal thoughts and of suicide attempts. Again, we can see in the figure that a higher proportion of undergraduate students have reported having suicidal thoughts and having attempted to end their lives.

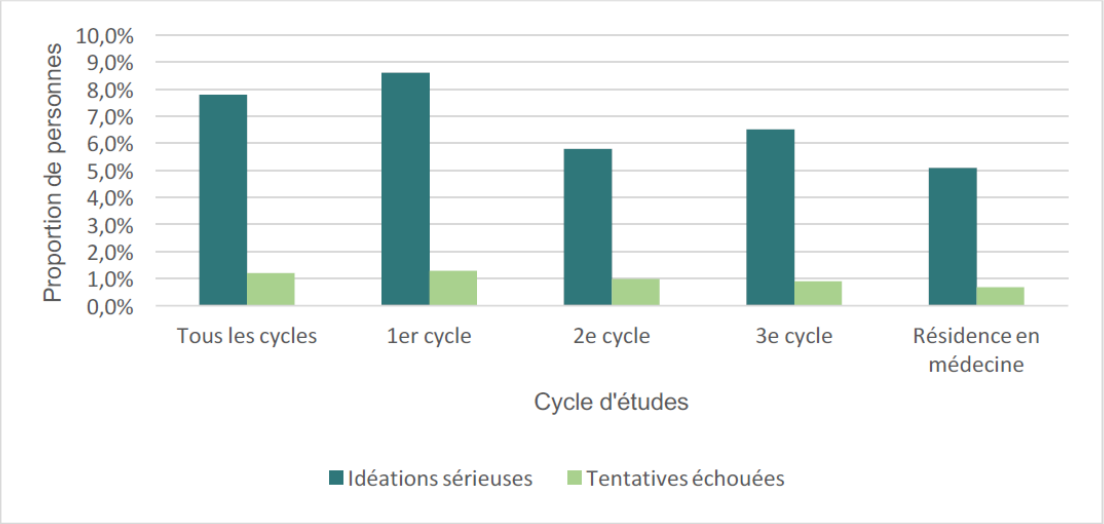

Figure 0.4. Percentage of people having serious suicidal thoughts (dark green) and failed suicide attempts (light green) for all cycle, undergraduates, master degree, doctoral degree and medicinal residency [translated from French, 3, fig. 4].

0.1.2. "Sous ta façade"

In 2018, the Quebec Student Union (UEQ) made a study of the mental well-being of its participating members (Bishop's University, ETS, HEC Montréal, ENAP, Polytechnique, UdeS, UQAC, UQAM, UQAR, UQTR, UQAT, ULaval and TÉLUQ) with 23 881 students representing 16.1% of the total student population of these schools [9]. The results were weighted to represent the entirety of the participating schools' members. This study was conducted using the same tests as in the "Ça va?" study and looked at the same four factors. Therefore, the study will help us see how the same factors affect mental health in students at other universities and we will also compare it to the general population of the same age.

Depression

In the UEQ study, they used the same PHQ-9 test as in the Faécum study. Comparing the results from those two, we see that 19% of respondents from UEQ study that presented symptoms severe enough to warrant an immediate treatment compared to 22% for Faécum study. Comparing Figures 0.1 and 0.5, we observe similar results from both studies for each cycle. We can also see that undergraduates are more likely to present symptoms of depression than graduate students. The UEQ study presents a very alarming case for the severity of depression symptoms for post-doctoral candidate with 25% of respondents showing severe symptoms.

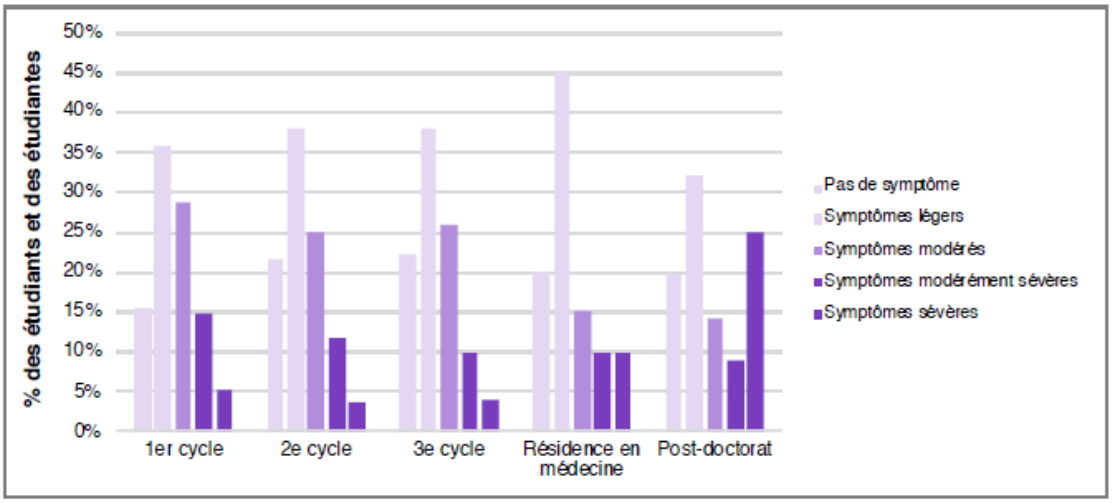

Figure 0.5. Percentage of people presenting symptoms of depression according to their level of study (all cycle, undergraduate, master level, doctoral study, medical residency and postdoctoral). The bars from left to right are no symptoms, light, moderate, moderately severe and severe symptoms [translated from French, 9, fig. 4].

Psychological Distress

For psychological distress, 58% of students from UEQ presented a score of 7 or higher compared to 64% of students from Faécum. In contrast, 20% of the general population had such a score [10].

The table 0.2 shows the results divided by age group on two different studies measuring psychological distress. We can observe that a higher percentage of students present high enough symptoms of psychological distress compared to the general population. We also see that younger age groups have a higher percentage than older ones.

Population	Province of Quebec	University students in Quebec
Year	2014-2015	2018
Age group	Proportions of population with a high level of psychological distress	
15-24	36.1	55.1
25-44	30.8	48.4
45-64	26.3	33.1

Table 0.2. Table comparing percentage of people from two studies having a high score on psychological distress test per age group [translated from French, 9, tab. 6].

Burnout

The third factor, burnout, was also measured with the same test as in the Faécum study. Contrary to the latter study, the UEQ study did not divide the results into 3 categories. They instead scaled the results from 0 to 30 with 30 representing the highest level of emotional burnout. This test does not have a threshold to indicate when someone is having severe symptoms of burnout or not. However, we can compare the average score of different groups among the total students sampled.

Figure 0.6 shows the average score on the burnout test per level of study. We can see that like previous factors, undergraduates are reporting having more symptoms than graduates.

Suicidal Ideation

In the Faécum study, we saw that the student population was more at risk of having suicidal thoughts or to report having attempted to take their life in the past 12 months. In the UEQ study, we see similar results with 7.7% of students reporting having serious suicidal thoughts during the last year of the study. To contrast, the proportion of the general population is 2.8%.

In table 0.3, we see the proportion of students having suicidal thoughts and that reported having attempted to end their life in the past 12 months divided by their level of study. Yet again we see an alarming number with 30.5% of post-doctoral candidates reporting having

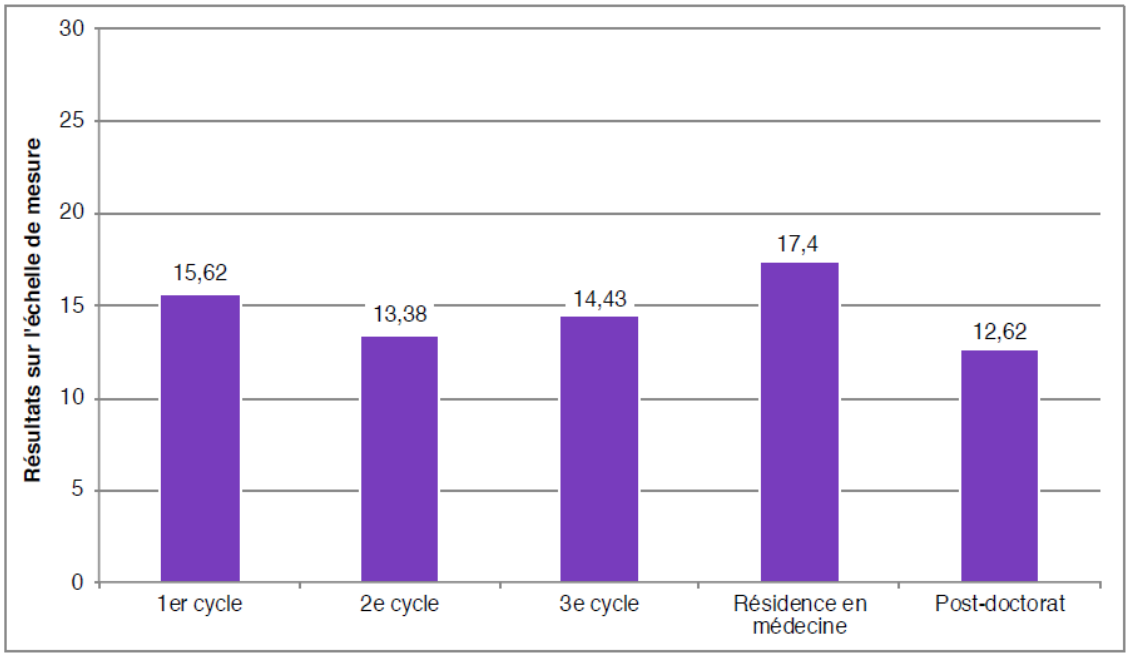

Figure 0.6. Mean score of each level of study (left to right: undergraduate, master, PhD, medical residency and postdoctoral) [translated from French, 9, fig. 6].

serious suicidal thoughts. We again see a bigger proportion of undergraduates showing signs of suicidal thoughts.

Level of study	Suicidal thoughts	Attempted suicide
Undergraduate	9.8%	1.1%
Master level	7.2%	0.6%
PhD level	5.8%	0.5%
Medical residency	12.4%	0.0%
Post-doctoral	30.5%	0.0%

Table 0.3. Table categorizing the proportion of students having suicidal thoughts and having attempted to end their life in the past 12 months per level of study [translated from French, 9, tab. 8].

In table 0.4, we see a comparison of the proportion of people per age group having suicidal thoughts and having attempted suicide from the general population, the Faécum study and the UEQ study. We can see that the younger the group age, the bigger proportion have had suicidal thoughts or had attempted suicide in the past 12 months.

Throughout those two studies, we saw that younger people are more at risk of showing symptoms of mental health problem relating to those four factors. When we look at the level of study, we see that undergraduates are also more likely to experience symptoms. That is

	Province of Quebec	"Ça va?"	"Sous ta façade"
Year	2014-2015	2016	2018
Age group	Proportion having suicidal thoughts in the past 12 months		
Total	2.8%	7.8%	7.7%
15-24	3.7%	7.8%	8.2%
25-44	3%	7.2%	7.7%
45-64	3.2%	5.3%	4.3%
65+	1.3%	0.0%	0.0%
Age group	Proportion having attempted suicide in the past 12 months		
Total	0.4%	1.2%	0.9%
15-24	1.0%	1.2%	1.3%
25-44	0.4%	1.1%	0.7%
45-64	0.3%	1.5%	0.1%
65+	0.2%	0.0%	0.0%

Table 0.4. Table categorizing the proportion of students having suicidal thoughts and having attempted to end their life in the past 12 months per age group [translated from French, 9, tab. 9].

likely due to their younger age with a mean age per cycle of 21.54 years old (undergraduate), 30.56 years old (master level) and 32.76 years old (PhD level) [11].

0.2. Impacts of mental health issues

Mental health problems are not a subject often talked about. Only recently did it begin to gain acceptance when athletes and other public figures shared their battle with mental illness. There is still a taboo about discussing mental health issues and a stigma even though its effects on our lives are very real. In this section, we will look at the impact of mental well-being on various aspects of our work and of our health.

0.2.1. Impacts on work

Mental health has a lot of effects on our work, whether it is on our productivity, performance or learning process. It is estimated that in 2010 the total cost of poor mental health on the world economy is approximately 2.5 trillion US dollars each year from sick leave and reduced productivity. That number is projected to reach 5 trillion in 2030 [12].

It is important to look deeper at how our productivity is affected by mental health. Studies show that our productivity slows down after a few hours of work [13, 14]. In other words, we only have a few hours of optimal productivity, after that it takes us more time to

accomplish our various tasks. There is a common belief that the output is linear as a function of hours worked, meaning that the more you work the more tasks you will accomplish. Contrary to that belief, studies have shown that this is not the case [13, 14]. Instead, they suggest that there is a maximum number of hours that we can work after which point there is a diminishing return in productivity. It is reduced by so much that we accomplish fewer tasks in total by working more hours. The Health of Munition Workers Committee even recommended in 1916 that the hours worked per week for men be limited to 65-67.

Figure 0.7 shows the maximum output of munition workers during the First World War. It was observed that the longer they worked the longer it took them to complete their tasks [14]. This observation is not only present in blue collared jobs but in white collared too. For white collared jobs, it also has the effect of reducing the performance of their work because of exhaustion [15, 16]. Stress and health levels (fatigue or health problem) can explain this reduction in performance. Overwork can often lead to burnout especially for chronic overtime (>60 hours a week). Burnout has been shown to negatively impact workers performance [17].

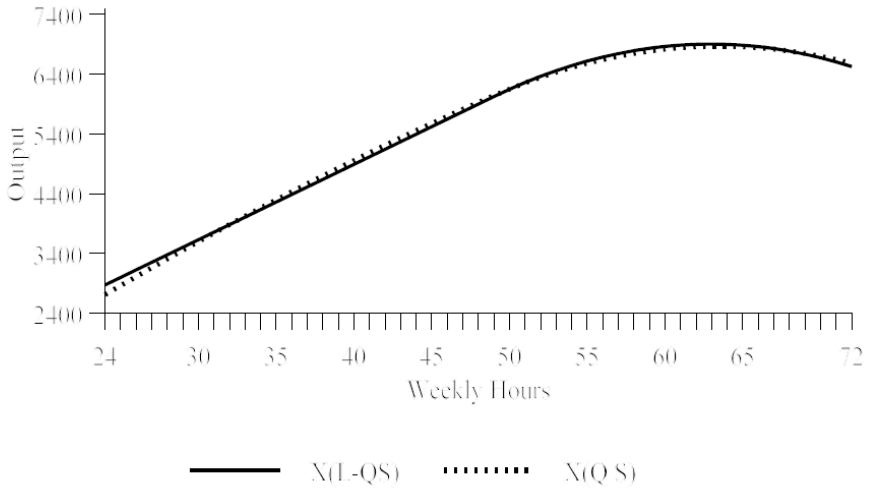

Figure 0.7. Output of munition workers during the First World War as a function of the number of hours worked per week. The two curves are fitted to all 122 weekly observations with the X(L-QS) having the first 49 hours fitted by a linear function and above 49 hours to a quadratic function. X(QS) being only fitted by a quadratic function [14, fig. 4].

There is a study that looked at the effect of working overtime and on weekends. They found that working at night and on weekends tends to deteriorate mental well-being of white and blue collared workers [18]. It can then be recommended for research group to limit, when possible, work during weekends and late at night. The same study also made a case that taking full holiday entitlement has a positive effect on mental stress. On a similar note, Iceland made trials to investigate a 4-day week workload. The preliminary results show

that it has a positive impact on the quality of life, work-life balance, on productivity and sometimes on total output per week [19]. The quality of service was also unaffected by this change.

Poor mental health is present in a good proportion of students as we saw in the previous section. Just like the impact on our works, it will also impact our concentration and the retention of information [20]. Studies have shown that stress has a negative impact on our cognitive capabilities [21, 22]. Stress can contribute to poor processing efficiency (meaning performance divided by effort) during exam because the high-anxiety individuals will have to use more processing resources than low-anxiety individuals. Other mental problems like depression can impair performance because depressed individuals will use some processing resources to their own concerns and therefore have less available for task performance. Therefore, a more stressful environment might lead to lower grades and be an obstacle to learning. Test anxiety is quite common with around 40% of students having moderate to high test anxiety [23]. Many causes for this anxiety are mental causes like fear of poor grades, using grades as a measurement of self-worth and placing too much importance on single test or work. An article from the University of Minnesota [24] showed that mixed assessment methods of evaluation closed the gap in gender overall performance in STEM. It can be recommended to use mixed assessment methods to reduce women attrition in STEM, which is already greater than men attrition. The same article also showed that exam performance gap was itself reduced when the weight of the exam was reduced in the overall grade. Consequently, students with test anxiety usually obtain half a letter grade below their peers in tests which corroborate the negative impact on cognitive capabilities.

Those capabilities can also be affected by the time of day the exam takes place. There is an article that looked at the average grade on an exam depending on the time of day it took place. We saw that the earlier it was during the day, the better the average grade was because students were not mentally drained by previous tasks earlier in the day [25]. This is inline with the optimal productivity in a day and how we only have a few hours to work to the best of capabilities that were previously mentioned.

Stress is only one element that affects the way students learn. The environment in which we study contributes significantly to the GPA of students. In fact, a study published in 2004 [26] showed that the amount of study of students is not a good predictor of their GPA. It only becomes significant when we consider the quality of study and previously attained performance. The quality of study can be affected by factors outside of the control of the students. For instance, the number of interruptions was negatively correlated with GPA [27]. A factor exacerbated by the COVID-19 pandemic for certain students who did not have access to quiet study place. Some also work to pay for their tuition. Studies [28, 29, 30] have shown that students who work less than 15 hours a week tend to have a higher GPA than students who don't work or work more than 15 hours. No study has been found

to look at the differences for different programs. An argument can be made that this result could differ for each program because of the difference in time spent studying. If a program requires more hours of study, then it is possible that working 10 hours a week might become the threshold. which would be logical following the maximum output per hours worked that were previously mentioned.

0.2.2. Impacts on physical health

There is a complicated relation between physical health and mental health. Physical injuries can negatively impact one's mental well-being and, conversely, mental illness can increase the risks of developing diseases. People with mental health issues are more at risk of being sleep deprived. Mental health issues have an impact on the quality of sleep and its duration [31]. This can lead to sleep deprivation in the long-term which in turn leads to difficulties concentrating, remembering information and learning [32]. This is another example of how poor mental well-being can negatively impact students and their grades or how the performance of workers is reduced after long-hour week. Mental health also increases the risks of developing various illnesses for examples diabetes, stroke and cardiovascular diseases [33]. It is because of many of those reasons that the study from Iceland saw that the four-day week workload leads to a better quality of life and reduced health risks. Such workload can also help gender equality because it allows a more equal share of family duties between both parents.

Mental health and overwork can have big impacts on our health. Looking at overwork is important because there are higher risks of developing mental health issues when we work long week workload [18]. An article from Japan [16] showed that people working more than 11 hours a day and those working more than 50 hours a week have increased risks of developing cerebra-cardiovascular diseases and myocardial infarction. They have also increased risks of developing hypertension, diabetes mellitus, depression, anxiety, and fatigue.

When we compare the developed countries where the number of hours worked is the lowest to the countries with the highest scores of happiness from the World Happiness Report of 2020 [34], we notice that 7 out of 10 are in both lists (Denmark, Iceland, Norway, Netherlands, Sweden, Luxembourg, and Austria). Many other factors can have an impact on the general happiness of a country. It is still interesting to see that there is a coincidence between the two. Why is happiness important from a business or a competitive research standpoint? Because we see that workers that are more motivated to go to work experience less stress and less fatigue than non-motivated workers [15], which in turn gives a boost in productivity.

0.3. Factors affecting mental well-being

When the situation of students' mental health is in this state and the lack of access to mental health resources is very difficult for students who can't afford it, it can become a crisis as it did in the University of Ottawa back in 2019. As a departmental unit, a research group or as a teacher, we can wonder what our options are to favor a better mental well-being for the students. In this section, we will look at the risk factors and the protection factor of mental well-being.

0.3.1. Risk factors

When measuring what factors contribute to mental health issues, studies do inferential analysis to determine whether there is a correlation between certain factors and a psychological issue. They look at the predictive power of a factor to determine a psychological issue. There are multiple factors that have been identified in the Faécum and UEQ studies: feeling of loneliness, financial insecurity, competition between peer, stress relating to redaction of memoirs or thesis, pressure to work over time during research, contribution in the projects of the research group, consumption of alcohol or drugs, ethnic minorities and sexual orientation [3]. Those factors have been ranked in the Faécum study from the most associated to negative mental health to the least shown in Table 0.5.

Ranking	Factors
1	Feeling of loneliness
2	Eating habits
3	Sleeping habits
4	Financial insecurity
5	Support by our peers
6	Possibility to fully express themselves
7	Competition between peers
8	Stress related to redaction
9	Too much difficulties in the research project or studies
10	Feeling of pressure to work late and/or during weekend
11	Contribution to research group projects

Table 0.5. Factors that are associated with negative mental health amongst students [3].

The feeling of loneliness is when you have this sense of solitude regardless of whether or not you spend a lot of time with other people. It can often stem from the perceived hostility of our environment and bring a feeling of seclusion from others. It is the factor most

related to negative mental health according to the Faécum study. The feeling of loneliness is the only factor that is associated with depression, burnout, psychological distress, and suicidal ideation amongst the student population [35]. Other factors such as the perception of financial insecurity can induce stress and are responsible for the variance of different mental illness symptoms. Financial insecurity is the 5th variable most associated to negative mental health. Its predictive factor is 73.8% and 60.0% for undergraduate and graduate students respectively. Meaning that those percentages of people having serious suicidal ideation could have been identified if we knew that they perceived to be in financial insecurity [3].

Competition between peers generally happens when students want to stand out because of their grade or inside their research group. It has been shown to have an inverse reaction to mental well-being. The more competition is present, the poorer the mental well-being is reported [36]. It can lead students to impostor syndrome, which the APA defines as "the situation in which highly accomplished, successful individuals paradoxically believe they are frauds who ultimately will fail and be unmasked as incompetent". Competition is the 7th variable most associated with the negative mental health indicators. Its predictive factors of suicide attempts are 58.6% and 28.4% for undergraduate and graduate students. Those factors for suicidal ideation are even higher than for financial insecurity. It goes to 74.2% and 64.2% for undergraduates and graduates respectively [3]. Stress related to redaction of memoirs or thesis, pressure to work overtime during research and the overall contribution in the projects of our research group are respectively the 8th, 10th and 11th variable most related to negative mental health. They are factors that are specific to graduate students and can be alleviated through support from the research group and adapted supervision. We will discuss more on that in the next section.

Consumption of alcohol or drugs are factors that are associated with a higher risk of poor mental well-being. Alcohol is often used as a self-medication. It helps alleviate stress and can have a positive impact. However, regular use of those substances can have a negative impact and heavy use is tightly tied to depression and suicidal ideation. The use of psychostimulants without ordinance is not well documented in research in Quebec. They can have serious side effects like hypertension, arrhythmia and even psychosis in case of an overdose. Being part of an ethnic minority or sexual orientation can also be a risk factor that can isolate an individual and cause a feeling of hostility from their environment. More inclusive measures should be taken to favor better mental well-being.

0.3.2. Protection factors

There are factors that have a tendency to aggravate mental health issues but others to prevent them. The protection factors will help prevent people from developing more severe

symptoms of mental health problems. Protection factors will help individuals to have more resilience when facing different issues.

Support by our peer is a strong factor both for undergraduate and graduate students that heavily influences the risk of an individual to develop symptoms of depression, psychological distress and suicidal ideation. It has a negative relation with mental illness symptoms. This support helps the individual's resilience when facing harder times. It can come from the support from other students in the research group or from the supervisor. Specifically, the supervision and the supervisor/student relation during the redaction of the thesis has a significant impact on the duration of a PhD [37]. Support by our peers is the fifth strongest factor explaining the variance of poor mental well-being. It explains 10.2% and 11.1% of variance for symptoms of depression for the undergraduate and graduate students respectively. Its potential to detect suicidal ideation is almost 60% for both levels of study [3]. The support by peers helps create a safe environment, especially for ethnic minorities and people with different sexual orientation. When the environment is safer, it allows the individual to fully express themselves. We call this the possibility of being authentic. It has a positive relation with mental well-being. This factor was only measured for the graduate students in the Faécum survey. It explains for 12.0% of the variance of symptoms of depression and can predict 67.7% of suicidal ideation [3]. Support by our peer and the possibility of being authentic are strong protection factors against depression and suicidal ideation.

We mentioned before the importance of sleep on the cognitive capabilities and our learning. It will not come as a surprise that long and good sleep is associated with better mental well-being. It is the third-strongest factor explaining the variance of symptoms according to the Faécum survey. It explains for 17.5% and 17.9% of variance among depression symptoms and it can predict 70.3% and 56.4% of suicidal ideation for undergraduate and graduate students respectively [3]. Having healthy eating habits is another healthy lifestyle that positively influences mental well-being. It is important to note that external factors for having healthy eating habits such as wishing to follow a perceived society's standard or even family dinner will instead have a negative impact on our mental well-being [38]. They will feel pressure to adjust to others' standard in fear of their judgment or their comments. Internal factors like wishing to live a healthier lifestyle will have a positive impact on their mental well-being. Nonetheless, healthier food has been found to help individual struggling with depression [39]. Combined with physical activities, they also have a positive impact of the management of stress.

Conclusion

In conclusion, we saw the current academic context and current research context negatively impact the students' well-being. These impacts in turn contribute to lower productivity, more difficulties in learning and can link to dangerous health issues. It is undeniable that a link exists between good mental well-being and the quality and quantity of work. It is now easier to talk about mental health struggle with our peers. Hopefully, this will lead academic institutions, departments or even professors to see more of the benefits of taking care of their students' mental well-being and they can have a constructive discussion about what can be done to do better. Mental struggle is a complex issue and there is so much more aspects that wasn't covered. It would be interesting to do a review of the impacts of various mental health services and their accessibility. Hopefully, one day things will get better. Until then, we need to keep our efforts to produce a better day.

References

[1] G. MacKean, "Mental health and well-being in postsecondary education settings", in *CACUSS pre-conference workshop on mental health*, 2011.

[2] K. Kroenke, R. L. Spitzer, and J. B. W. Williams, "The PHQ-15: validity of a new measure for evaluating the severity of somatic symptoms", *Psychosomatic medicine*, vol. 64, no. 2, pp. 258–266, 2002.

[3] F.-E. Lessard *et al.*, "Enquête sur la santé psychologique étudiante", *Fédération des associations étudiantes du campus de l'Université de Montréal*, 2016.

[4] R. C. Kessler *et al.*, "Screening for serious mental illness in the general population", *Archives of general psychiatry*, vol. 60, no. 2, pp. 184–189, 2003.

[5] C. Maslach, S. E. Jackson, and M. Leiter, *Maslach Burnout Inventory Manual*, 3rd ed. Palo Alto, CA: Consulting Psychologists Press, Inc, 1996.

[6] M. Fleury and G. Grenier, "État de situation sur la santé mentale au Québec et la réponse du système de santé et de services sociaux", *Commissaire à a la santé et au bien-être du Québec*, 2012.

[7] M. Morasse, *L'université d'Ottawa secouée par une vague de suicides*, Last accessed on 2 December 2021, 2020. [Online]. Available: `https://plus.lapresse.ca/screens/9150fb84-f945-4bdc-9760-1028e0ae41a1__7C___0.html`.

[8] S. Yogaretnam, *Five Student Deaths in 10 months: UOttawa faces mental health crisis*, Last accessed on 2 December 2021, 2020. [Online]. Available: `https://ottawacitizen.com/news/five-student-deaths-in-10-months-uottawa-faces-mental-health-crisis`.

[9] J. Bérard *et al.*, "Sous ta façade", *Union étudiante du Québec*, 2018.

[10] Institut de la statistique du Québec, *L'Enquête québécoise sur la santé de la population 2014-2015: pour en savoir plus sur la santé des Québécois [et des Québécoises]*, 2016. [Online]. Available: `http://www.stat.gouv.qc.ca/statistiques/sante/etatsante/sante-globale/sante-quebecois-2014-2015.html`..

[11] Statistique Canada, *Les tendances de la composition selon l'âge des étudiants et des diplômés collégiaux et universitaires*, Last accesssed on 7 December 2021, 2007. [Online]. Available: `https://www150.statcan.gc.ca/n1/pub/81-004-x/2010005/article/11386-fra.htm`.

[12] S. Trautmann, J. Rehm, and H.-U. Wittchen, "The economic costs of mental disorders", *EMBO Rep*, vol. 17, pp. 1245–1249, 2016.

[13] M. Collewet and J. Sauermann, "Working Hours and Productivity", *IZA DP*, no. 10722, 2017.

[14] J. Pencavel, "The Productivity of Working Hours", *IZA DP*, no. 8129, 2014.

[15] D. G. J. Beckers *et al.*, "Working overtime hours: Relations with fatigue, work motivation, and the quality of work", *PubMed*, 2004.

[16] K. Wong, A. H. S. Chan, and S. C. Ngan, "The Effect of Long Working Hours and Overtime on Occupational Health: A Meta-Analysis of Evidence from 1998 to 2018", *Int. J. Environ. Res. Public Health*, vol. 16, 2019.

[17] G. Pan, "The Effects of Burnout on Task Performance and Turnover Intention of New Generation of Skilled Workers", *Journal of Human Resource and Sustainability Studies*, vol. 5, pp. 156–166, 2017.

[18] K. Sato, S. Kuroda, and H. Owan, "Mental health effects of long work hours, night and weekend work, and short rest periods", *Social Science & Medicine*, no. 246, 2020.

[19] G. D. Haraldsson and J. Kellam, *Going Public: Iceland's Journey to a Shorter Working Week*, Last accessed on 20 December 2021, 2021. [Online]. Available: `https://autonomy.work/wp-content/uploads/2021/06/ICELAND_4DW.pdf`.

[20] Division of Sleep Medicine at Harvard Medical School, "Sleep, Learning and Memory", 2007, Last accessed on 20 December 2021. [Online]. Available: `https://healthysleep.med.harvard.edu/healthy/matters/benefits-of-sleep/learning-memory`.

[21] M. W. E. M̃. G. Calvo, "Anxiety and Performance: The Processing Efficiency Theory", *Cognition & Emotion*, vol. 6, no. 6, pp. 409–434, 1992.

[22] P. W. Ellis H. C. & Ashbrook, "Resource allocation model of the effects of depressed mood states on memory", *K. Fiedler & J. Forgas (Eds), Affect, cognition and social behaviour. Toronto: Hogrefe.*, 1988.

[23] Oxford Learning, *What is Test Anxiety (and How It Affects Students)*, Last accessed on 3 January 2022, 2018. [Online]. Available: `oxfordlearning.com/what-is-test-anxiety`.

[24] S. Cotner and C. J. Ballen, "Can Mixed Assessment Methods Male Biology Classes More Equitable?", *PLoS ONE*, vol. 12, no. 12, 2017.

[25] H. H. Sievertsen, F. Gino, and M. Piovesan, "Cognitive fatigue influences students' performance on standardized tests", *PNAS*, no. 10, pp. 2621–2624, 2016.

[26] E. A. Plant *et al.*, "Why study time does not predict grade point average across college students: Implications of deliberate practice for academic performance", *Contemporary Educational Psychology*, vol. 30, pp. 96–116, 2004.

[27] G. J. Allen, W. M. Lerner, and J. J. Hinrichsen, "Study Behaviors and Their Relationships to Test Anxiety and Academic Performance", *Psychological Reports*, vol. 30, no. 2, pp. 407–410, 1972.

[28] L. Dundes and J. Marx, "Balancing Work and Academics in College: Why Do Students Working 10 to 19 hours per Week Excel?", *J. College Student Retention*, vol. 8, pp. 107–120, 2006.

[29] S. A. Nonis and G. I. Hudson, "Academic Performance of College Students: Influence of Time Spent Studying and Working", *Journal of Education for Business*, vol. 81, no. 3, pp. 151–159, 2006.

[30] J. Okogbaa, R. E. Allen, and D. F. Sarpong, "Time Spent at Work and Its Impact on the Academic Performance of Pharmacy Students", *Int. J. Environ. Res. Public Health*, vol. 17, no. 2, 2020.

[31] M. Wainberg *et al.*, "Association of accelerometer-derived sleep measures with lifetime psychiatric diagnoses: A cross-sectional study of 89,205 participants from the UK Biobank", *PLoS Med.*, vol. 18, no. 10, 2021.

[32] E. Suni, *How Lack of Sleep Impacts Cognitive Performance and Focus*, Last accessed on 5 January 2022, 2020. [Online]. Available: `https://www.sleepfoundation.org/sleep-deprivation/lack-of-sleep-and-cognitive-impairment`.

[33] U.S. Department of Health and Human Services, "Chronic Illness and Mental Health: Recognizing and Treating Depression", *NIH Publication*, no. 21, 2021.

[34] United Nations, *World Happiness Report 2020*, Sustainable Development Solutions Network, 2020.

[35] S. Lupien, "La solitude des étudiants universitaires", *Revue DIRE*, vol. 28, no. 2, 2019.

[36] J. K. Hyun *et al.*, "Graduate student mental health: Needs assessment and utilization of counseling services", *Journal of College Student Development*, vol. 47, no. 3, 2006.

[37] M. Le *et al.*, "The impacts of supervisor - PhD student relationships on PhD students' satisfaction: A case study of Vietnamese universities", *Journal of University Teaching & Learning Practice*, 2021.

[38] J. Polivy *et al.*, "Mental health and eating behaviours: a bi-directional relation", *Can J Public Health*, 2005.

[39] J. Clarke, *Foods to Help Fight Depression*, Last accessed on 9 January 2022, 2020. [Online]. Available: `verywellmind.com/foods-for-depression-4156403`.

Introduction

The Standard Model of particle physics has long been known to be incomplete. Many different theoretical problems cannot be explained solely by it. One such problem is the existence of dark matter. Even after almost 90 years since it was first proposed, dark matter has never been observed conclusively. Many collaborations have tried for decades to simply get a glimpse at what it could be and how it would interact with the particles of the Standard Model.

At a time when dark matter detectors are starting to have enormous sizes, many questions surrounding their use and functionality are still unanswered. Among the ton-scale generation of dark matter detectors, PICO-500 will have unparalleled sensitivity to spin-dependent dark matter interactions.

In this work, we will try to answer a pressing question regarding the sensitivity of PICO-500. To aid the thermal design of PICO-500, a mixture of perfluorocarbons may be used. Existing calculations to predict the sensitivity of bubble chambers filled with pure liquids may not apply to such a mixture. We will test whether the Seitz nucleation model works for mixtures.

Chapter 1 will focus on some evidence of dark matter and some of the popular particle models to describe dark matter. The theory of bubble nucleation will be described which will lay the foundation for the use of a bubble chamber for dark matter detection. In Chapter 2, a more detailed explanation of a PICO bubble chamber will be presented. In Chapter 3 will present the acquired data, followed by results and comparisons to the Seitz model in Chapter 4.

Chapter 1

Dark Matter Detection with Bubble Chambers

This chapter will present evidence for the existence of dark matter. These measures constrain dark matter models. The most promising such models will be presented. These motivate the direct detection of dark matter in the PICO experiment using bubble chambers. Finally, the Seitz Model, which describes how a bubble chamber can search dark matter, will be presented.

1.1. Dark Matter

It has been proposed that dark matter composes approximately 85% of matter in our universe, but it has not yet been conclusively observed. It would be normal to ask ourselves why we think it exists and what form it would take. It is called dark because it does not interact or very weakly interact with light and by extension the electromagnetic force. This means that we couldn't see it by conventional means. However, we can see its gravitational impact on regular matter which shows that there is something beyond our current knowledge.

1.1.1. Evidence of Dark Matter

The existence of dark matter allows us to explain a number of astrophysics phenomena like galaxy rotation curves, the shape of the bullet cluster and the baryon acoustic oscillations. Scientists have used those phenomena to constraint dark matter candidates.

Galaxy Rotation Curves

In 1933, Fritz Zwicky studied the velocity distribution in the Coma cluster [1]. Using the virial theorem, he estimated that the cluster needed to be 400 times more massive than it was in order to explain the velocities measured. He suggested that an invisible matter (or dark matter) could justify this discrepancy. In took until the 1970s for his proposal to

gain support. Vera Rubin studied the rotational velocities of stars around the center of their galaxy using the Doppler effect [2]. From Newtonian mechanics, the velocity of a star, v, should follow equation 1.1.1,

$$v = \sqrt{\frac{GM(r)}{r}}, \tag{1.1.1}$$

where G is the gravitational constant, $M(r)$ is the sum of the mass of the stars from the galactic center to a radius r. If the star is far from the galactic center, then $M(r) \approx M_{gal}$, the mass of the galaxy. Thus, the velocities should be proportional to $\sqrt{1/r}$. Figure 1.1 shows the experimental data from the galaxy NGC 6503 and the theoretical curve from Newtonian mechanics. We can see that at low radius, there is a good accordance between data and the theory including only the star disk. However, at large radius from the galactic center, we would expect the velocities to fall off as seen in the star disk curve, but instead it stays constant. This is what Rubin noticed. It was proposed that a spherically symmetrical halo of dark matter was surrounding the galactic center, gravitationally affecting the furthest stars to produce this velocity distribution. This gives us two criteria for a dark matter candidate. It doesn't interact with light and it has a mass.

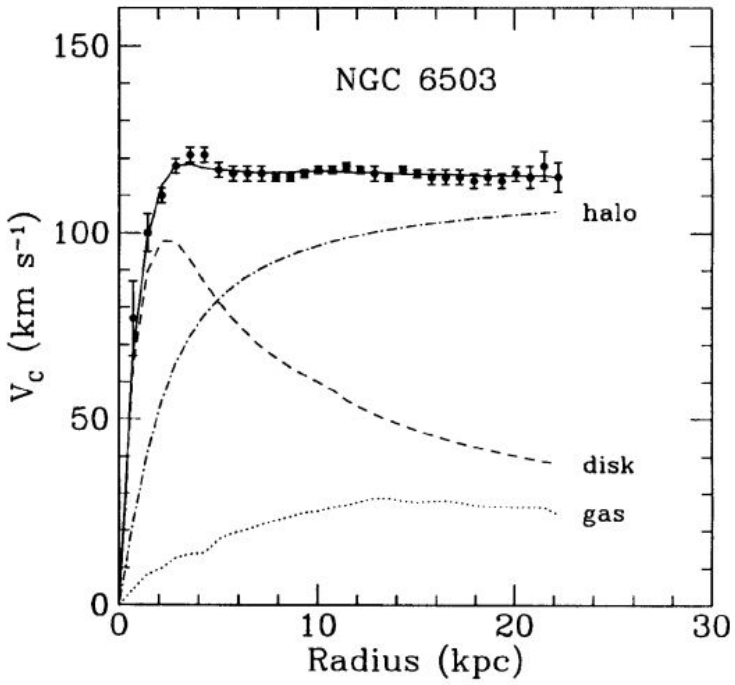

Figure 1.1. Velocity distribution of stars around the galactic center of NGC 6503 (data points) and the velocity distribution from Newtonian mechanics based on the total contribution of gas, star disk and dark matter halo (solid lines) [3]. The other curves are fits of the mass contribution from the star disk, the baryon gas and the dark matter halo to fit the data.

Bullet Cluster

The bullet cluster also known as 1E 0657-56 is a collision of two galaxy clusters situated at a comoving distance of 1.141 Gpc [4]. In Figure 1.2, we can see its luminous mass by looking at the X-ray spectrum and the mass distribution measured through gravitational lensing. The vast majority of the luminous mass is made of gas. The mass distribution measured through gravitational lensing is the real mass distribution of the cluster. We can observe a significant difference between the two. What we can see is that the luminous mass is situated at the center because of the collision, and the majority of the mass of the cluster is spread out away from the center similar to a collision-less galaxy. This suggests that the dark matter which composes most of the total mass has not really interacted with the other particles. This provides another criterion for a dark matter candidate that it should weakly interact with other particles from the Standard Model and with itself.

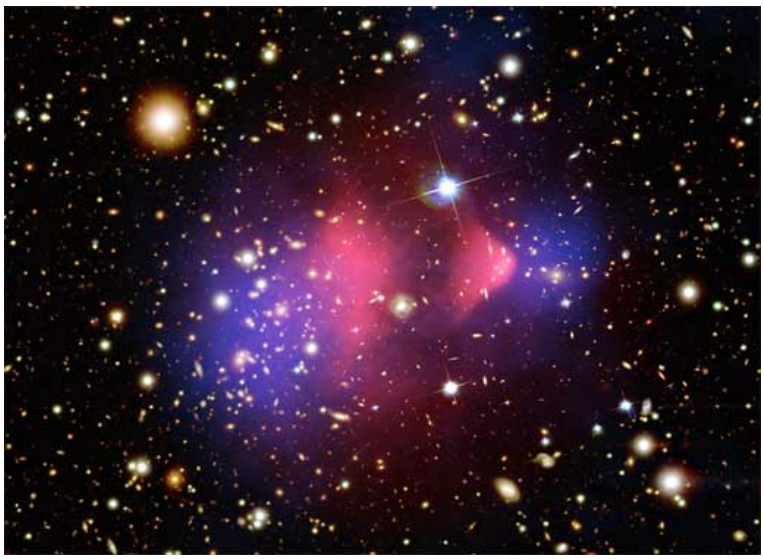

Figure 1.2. Composite image of the Bullet cluster [5, 6]. In pink is the Chandra X-ray Observatory picture and in blue is the matter distribution calculated through gravitational lensing.

Baryon Acoustic Oscillations

Ever since the Big Bang, the Universe has been expanding, cooling and reducing in density. During the period where the charged particles and the photons were still of equal density, a pressure coming from the thermal coupling was exerting an outward force from regions of overdensity that moved the particles. At some point, the particles were so sparse that baryons, electrons and photons decoupled. The baryons then were attracted because of gravity while the photons continued outward leading to the cosmic microwave background radiation. The pressure from the thermal coupling and the force from gravity created a wave

within the baryon density called baryon acoustic oscillation. In Figure 1.3, we can see a visual representation of the rapid expansion around the initial clumps shortly after the Big Bang. The remnants of this acoustic wave can still be found today as shown by Eisenstein et al. in Figure 1.3 [7]. The bump at around 100 Mpc represents a deviation from the uniform density of the universe. This anisotropy would be caused by the baryonic acoustic oscillations. If we try to simulate the baryon acoustic oscillation assuming a model of only baryons and photons, we cannot explain their results if we take into account the age of the Universe and the measured densities of charged particles and photons. There would need to be a lot more mass that rapidly decoupled from the baryons and photons. It was proposed that dark matter is this missing mass that was produced during or after the Big Bang and helped shape the galaxies that we now see. Since we can also see the effect of dark matter today, this adds another criterion that the candidate should be stable.

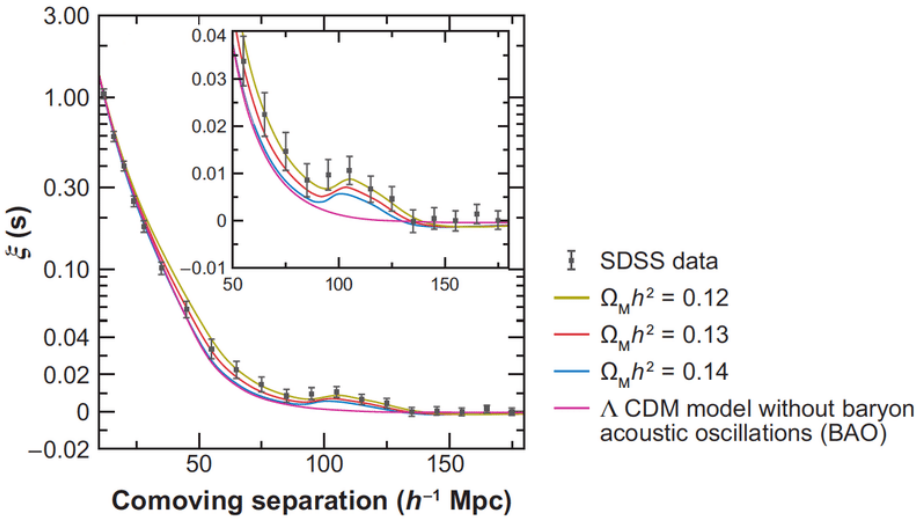

Figure 1.3. Correlation function from Eisenstein et al. [7, fig. 2] describing the deviation from uniform density. The data points were made using the Sloan Digital Sky Survey data. The various curves represent different levels of baryon density in the Universe.

1.1.2. Dark Matter Model

Many theorists have tried for decades to find a model to explain dark matter. They made simulations to attempt to fit their model with the experimental data and reject some of them. A widely circulated drawing amongst the dark matter physicists can be found in Figure 1.4 that presents some of the models that theorists proposed in order to explain the dark sector. We will focus on the two most popular candidates: the WIMPs and the axion.

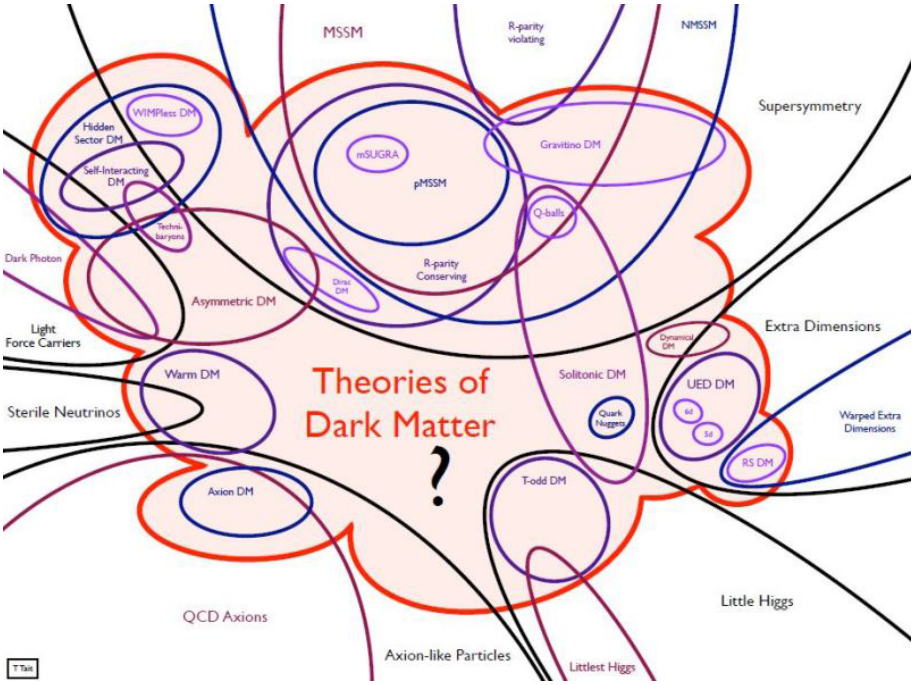

Figure 1.4. Venn diagram of the dark sector and its many dark matter models [8].

WIMPs

Weakly interacting massive particles are a category of particles that interact solely with gravity and either the Standard Model weak force or another force yet to be known. The mass of WIMPs should be between 2 GeV/c^2 and 100 TeV/c^2 [9]. Many dark matter candidates can be put in this category, but there is one that really stands out, the neutralino.

Many theories predict the existence of WIMPs. One class of such theories is the Supersymmetric Standard Model. In these, each known fermion is associated with a new boson with 1/2 spin difference and, vice versa, each known boson is associated with a new fermion. This association is called superpartner. It would effectively double the number of particles in the Standard Model. The lightest particle from the minimal SUSY would be the neutralino, a neutral spin 1/2 particle. It would be a linear combination of two higgsinos, a photino and a zino, the superpartners of the Higgs boson, the photon and the Z boson respectively. If we assume a conservation of R-parity, the neutralino would be a stable particle since it cannot decay into lighter particles without violating this conservation. This particle checks out two of the criteria previously mentioned for a dark matter candidate. The fact that a particle fitting the necessary criteria for dark matter naturally comes from the SUSY model is often called the WIMP miracle.

Dozens if not hundreds of experiments like PICO, SuperCDMS and LUX are trying to directly detect the WIMPs. While the exact nature of the dark matter interaction is yet to be known, we know two types of interaction: spin-dependent and spin-independent. The

neutralino having a 1/2 spin can have a spin-spin interaction with a nucleus. Therefore, SuperCDMS detectors made of germanium or silicon are only sensitive to the spin-independent interaction while PICO detectors containing carbon and fluorine atoms are sensitive to both. Another mechanism for the discovery of dark matter would be through its production at colliders such as the LHC. Since dark matter should only weakly interact with Standard Model particles, we would see a large amount of missing momentum. The LHC has observed neither any supersymmetric particle nor any notable excess of jets or leptons with missing energy [10]. Some experiments like Fermi LAT and IceCube are instead looking for indirect detection through the annihilation of neutralino. This annihilation could produce an excess of photons or neutrinos at the mass energy of the neutralino or any particle below that energy. Since this annihilation has not been observed conclusively combined with the total amount of dark matter, we can assume that the annihilation cross section must be very low.

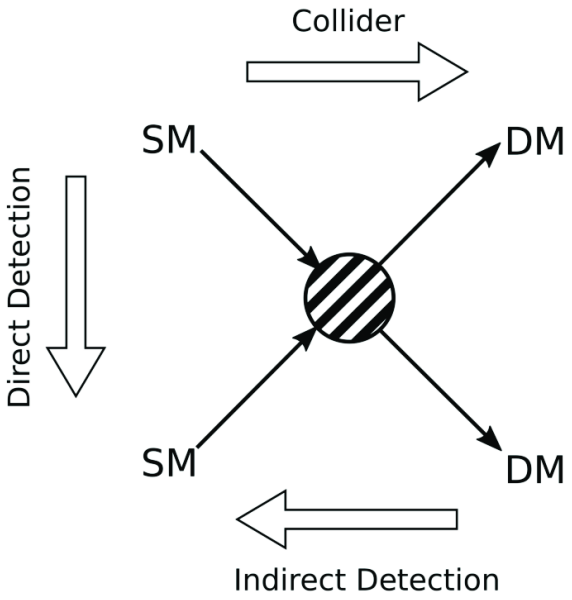

Figure 1.5. Feynman diagram representing the direct, indirect and production of dark matter depending on the time direction and how they all relate to the same effective interaction [11].

Axion

Charge-parity (CP) violation was first observed for the weak nuclear force through kaon decay. The electromagnetic force conserves this symmetry. Experimentally, the strong nuclear force also conserves this symmetry but the Standard Model doesn't explicitly prevent CP violation. In 1977, Roberto Peccei and Helen Quinn [12] proposed a new symmetry for the strong force, now named after them. This Peccei-Quinn symmetry would spontaneously

break, creating a boson with a very low mass, solving the CP violation problem. This particle was called axion. It doesn't have a charge and its spin is 0. Its mass would range from 1 μeV/c^2 to 1 eV/c^2.

The axion has different interacting processes than the neutralino. Instead, axions could interact via the Primakoff effect [13], where the axions are transformed into photons in a strong magnetic field. Since its mass is so low, it would prevent the axion from decaying into other particles. Many experiments like ADMX and CAST are looking for axions. Other experiments like SuperCDMS and EDELWEISS are also sensitive to axion, however, to a lesser extent since their main goal is the detection of WIMPs.

1.2. Seitz Model

In 1952, Donald Glaser invented a superheated liquid detector called a bubble chamber to measure charged particles. The idea was to heat a liquid just below its boiling point and become superheated. When a charged particle passes through the chamber, it would vaporize the superheated liquid and create microscopic bubbles along its track. Glaser won the Nobel Prize for Physics in 1960 for his invention. In the pursuing years after his invention, he tried to explain bubble formation in bubble chambers with an electrostatic theory, but ultimately failed. Following discussions with Glaser, Frederick Seitz published a paper in 1958 called *On the Theory of the Bubble Chamber* [14] where he first laid out an explanation of the bubble nucleation inside bubble chamber, that we use today to describe PICO.

1.2.1. Hot spike model

The original view of the production of a bubble in a bubble chamber was that it was associated with the production of free electrons from the ionization. Seitz in his paper proposed that it was due to the production of "highly localized hot regions" paving the way for the hot spike model. In this model, a particle deposits a fraction of its energy through elastic scattering with a nucleus. This creates a short-range recoil that produces this hot spike. This also means that it does not require that the particle have a charge. Neutral particles like neutrons or even neutrinos can elastically interact with a nucleus and create a hot spike. However, certain criteria are needed to be met for an interaction to induce a bubble nucleation.

1.2.2. Critical radius

Consider a bubble of radius r produced by a point-like energy deposition. This bubble will have three main forces applied on it: the force associated with the gas pressure (pressure inside), the force associated with the liquid pressure (pressure outside) and the surface tension. In Figure 1.6, we can see that the gas pressure (blue arrow) has an outward force

while the liquid pressure (red arrow) and the surface tension (green arrow) have an inward pressure.

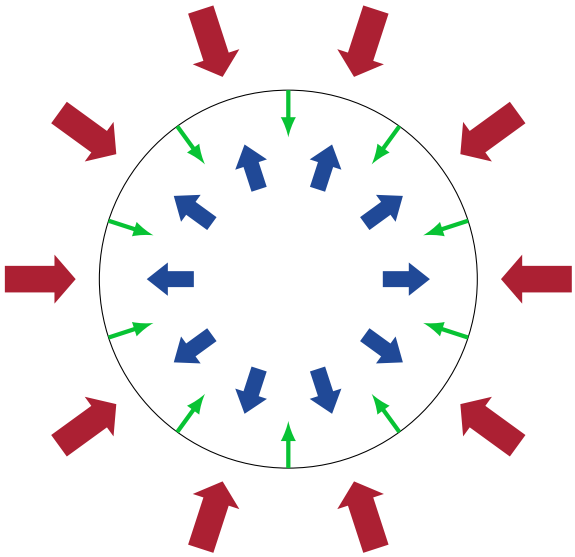

Figure 1.6. Forces on a bubble. In red is the liquid pressure, in blue is the gas pressure and in green is the surface tension.

We can write an equation of the sum of those forces seen in equation 1.2.1,

$$p_g dV - p_l dV = \sigma dA, \tag{1.2.1}$$

where $p_g dV$ and $p_l dV$ are the work done by the gas pressure, p_g, the liquid pressure, p_l, pressure respectively and σ is the surface. The work done by the surface tension is σdA. By replacing $dV = 4\pi R^2 dR$ and $dA = 8\pi R dR$, it is possible to find a critical radius, R_c, where the bubble will be at an unstable equilibrium given by the equation 1.2.2.

$$R_c = \frac{2\sigma}{(p_g - p_l)}. \tag{1.2.2}$$

The instability of this equilibrium means that a bubble of smaller radius will collapse while a bubble of larger radius will expand. It also provides us with a first criterion for a complete phase transition. The work done by the gas pressure must to be more than the work of the liquid pressure and the surface tension for bubbles to be created.

1.2.3. Critical energy and Seitz criteria

It is more convenient to put the critical radius in terms of the energy necessary to induce an irreversible phase transition. We call it the critical energy, E_c. With the previous equations, the critical energy becomes:

$$E_c = \frac{4\pi}{3}R_c^3(p_l - p_g) + \frac{4\pi}{3}R_c^3(h_v(T) - h_l(T)) + 4\pi R_c^2\left(\sigma - T\frac{d\sigma}{dT}\right) + W_{irr}, \tag{1.2.3}$$

where $h_v(T)$ and $h_l(T)$ are the latent heat of the gas and the liquid respectively. The first term represents the work needed to form the critical bubble. The second term represents the work needed for a phase transition from liquid to gas. The third term represents the work done to compensate the surface tension. The fourth term, W_{irr}, is the irreversible work from the acoustic emission.

The critical energy is dependent on the liquid temperature, T, through the latent heat and the surface tension terms. It is also dependent on the liquid pressure, p_l, through the first term. By changing the temperature and the pressure of the liquid, it is possible to set a particular threshold energy required to form a bubble.

The critical energy provides us with a second criterion for the complete phase transition. It is not enough that the energy deposited be above the critical energy. It also needs to be deposited on a small enough distance that it will induce a complete phase transition (eq. 1.2.4).

$$\frac{dE}{dx}L_c > E_c, \tag{1.2.4}$$

where $L_c = bR_c$ is the critical length, b is the Harper parameter that is found experimentally and $\frac{dE}{dx}$ is the stopping power. If the stopping power deposited over a certain distance is higher than the critical energy, than a bubble will form. Molecular dynamics simulations can be used to model this stopping power threshold [15], but historically, the case of an infinitely long track was considered.

In bubble chamber, there is a response from the detector which is described as a probability of nucleation. This probability will be described by a 5-point function. This function will be explained in more details in section 2.3. The recoil energy needs to be higher than the threshold energy ($E_r > E_{th}$) in order for a bubble nucleation. We can use this probability to calculate the observed count rate, R_{obs}.

$$R_{obs} = \int_0^{E_{r,max}} P(E_{th}, E_r)\frac{dR}{dE_r}dE_r, \tag{1.2.5}$$

where we integrate over every recoil energy. This observed count rate can help us find the cross section for a particular interaction. The total rate observed is the sum of the rate on all carbon and fluorine atoms.

1.2.4. Seitz Model for mixture

The Seitz model for mixture has some differences with the model for pure fluid. For instance, the diffusion of each fluid through the surface of a bubble may not be equal,

meaning that the critical radius may shift as a function of time. Two limiting cases for our study are the mass transport across the phase surface and proportion of each fluid in the bubble compared to their proportion in the liquid. It was assumed in the Seitz threshold calculation that the proportion was the same in both liquid and the bubble. We also assume that the gas composition is at equilibrium and that the entire neutron energy is given to the gas so there is no thermal exchange between the gas and the liquid during the bubble growth. As previously mentioned, the Seitz threshold for a superheated liquid depends on its pressure and its temperature. The threshold will also vary from one liquid to another at fixed temperature and pressure. Using a mixture of liquid, we can vary the Seitz threshold depending solely on the ratio of each liquid. An application of this can be seen in Figure 1.7 where we see a curve of the temperature required to obtain a Seitz threshold of 3 keV at 30 psi of pressure as a function of the fraction of C_3F_8 in a mix of C_3F_8 and C_4F_{10}.

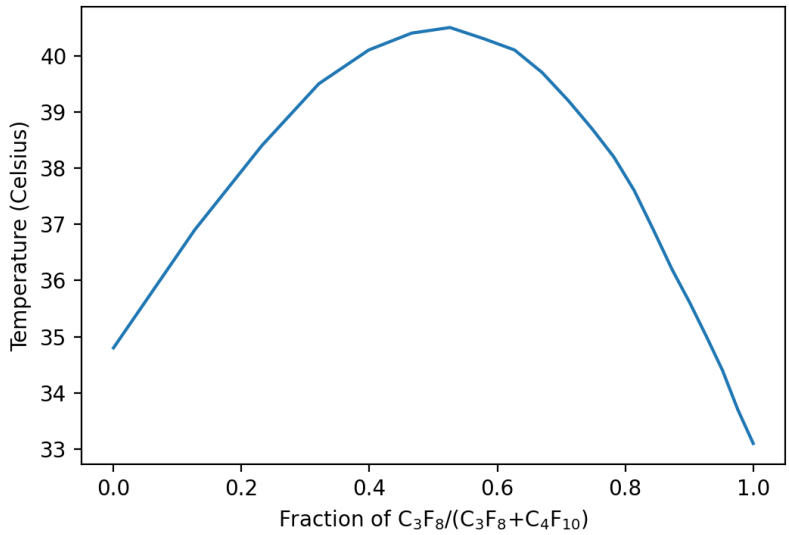

Figure 1.7. Curve of the temperature to obtain a 3 keV Seitz threshold at 30 psi as a function of the fraction of C_3F_8 in a mix of C_3F_8 and C_4F_{10} [16].

1.3. Context of this Work

Bubble chambers have been used in various particle physics experiments such as Gargamelle, PICASSO, COUPP and PICO. The latter three use perfluorocarbon refrigerant as a working medium. The work presented in this thesis was done in collaboration with the PICO experiment. The latest prototypes of PICO detectors are designed with a cold inactive and a hot active region. The temperature at which either region will be set depends on the perfluorocarbon used, as described in section 1.2.4. It was proposed that by using a mixture of two perfluorocarbons, the operating temperature of the detector could be set by

choosing the ratio of the perfluorocarbons. This ability to choose the operating temperature relaxes the thermal design requirements for large bubble chambers by having one of the regions being controlled at ambient temperature while the other region could be warmed up. The results presented will help the collaboration in their design.

This thesis will focus on the calibration of a perfluorocarbon mixture of C_3F_8 and C_4F_{10}. Many others have done similar experiments using the PICO-0.1 detector, but only with pure perfluorocarbon. Guillaume Giroux [17] measured the bubble count rate as a function of threshold energy with neutrons in C_3F_8, Simon Chen [18] measured the nucleation from a gamma source on C_3F_8 and Frederic Tardif [19] characterized the Seitz threshold for the pure C_2ClF_5 and pure $C_2H_2F_4$. The goals of our analysis are similar to those Tardif, but will use newer analysis techniques developed by other PICO collaboration members.

Chapter 2

The PICO Experiment

In this chapter, we are going to explain how a bubble chamber operates. We will then explain how the various systems of the PICO-0.1 detector works, specifically how a neutron can be used to simulate a dark matter signal and how it will interact in a bubble chamber to produce a bubble. A description of the particle accelerator used will be made and the target used to produce the monoenergetic neutron through resonant reactions. The mixing procedure to obtain the perfluorocarbon mixture will be detailed.

2.1. Bubble chambers

Bubble chamber detectors were instrumental in the discovery of the weak neutral current at the Gargamelle experiment and ultimately set the stage for the discovery of the W and Z bosons. They use a smooth-surfaced container which is filled with an active fluid. The pressure and the temperature of this fluid are controlled in order to achieve a superheated liquid state. Usually, only one of the two is used as a free parameter while the other is maintained constant. When a bubble is formed, sensors like a camera or piezoelectric sensor are used to detect it. The detector changes the free parameter to return in a completely liquid state to crush the bubble. After returning to equilibrium, the system is returned to the superheated state ready for another event.

The PICO detectors use the expertise with acoustic signals developed by the PICASSO experiment combined with the detection techniques from the COUPP experiment. Their combined design used an entire jar filled with superheated perfluorocarbon as its active element which was a major improvement from PICASSO detectors who could only use $\sim$2% of the total volume as active element. The expertise of the PICASSO experiment on the acoustic signals from the bubble was further developed to better discriminate between the various particles interacting with the chamber. In this work, the PICO-0.1 detector was used and a detailed description will be made.

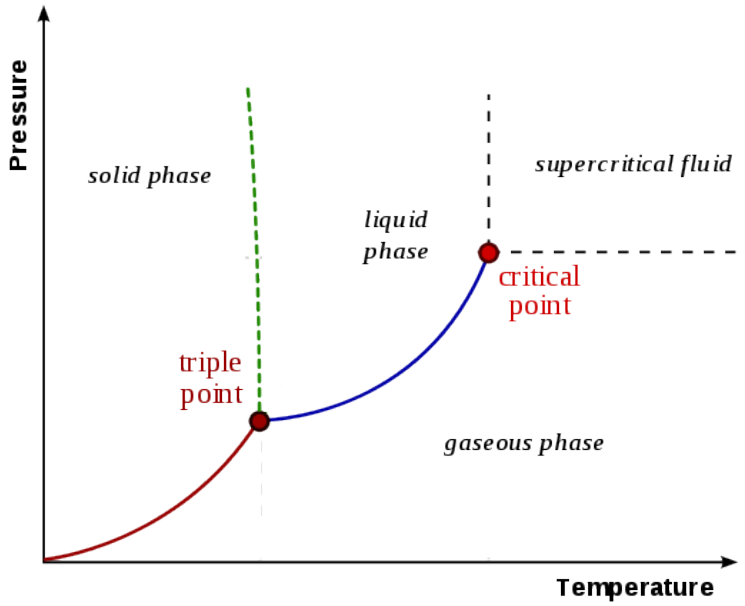

Figure 2.1. Phase state diagram. The blue line represents the saturation line where the fluid is supposed to be a gas but instead stays a liquid until enough energy can induce a phase transition following the Seitz model [20].

2.2. PICO-0.1

PICO-0.1 is a calibration prototype mainly used to test different refrigerant fluids and their Seitz threshold. Its inner vessel has a form similar to a test tube with a volume of 75 mL made of XQ-80, a high purity quartz reaction vessel made by Cole-Parmer. The inner vessel was filled with a mixture of C_3F_8 and C_4F_{10}. The electronic and the data acquisition system (DAQ) was designed by members of the COUPP collaboration. We can see in Figure 2.2 the various systems of the PICO-0.1 detector: the temperature system (not shown), the hydraulic pressure system and the cameras.

2.2.1. Temperature system

The temperature of the detector was controlled by a recycling chiller connected to a bath as seen in Figure 2.3. This chiller was able to control the temperature to a precision of 0.1°C, verified by 3 resistance temperature detectors (RTD) measurements. The cooled distilled water is pushed through a tube connected in the middle of the base of the water bath. The detector was cooled by this water from the bottom up. The water was brought back to the chiller through an overflow tube located at the top of the bath. This tube is connected back to the chiller where the water is cooled once again before starting a new cycle through the chilling system. The speed of the cycle is mainly determined by the diameter of the overflow tube since there is a maximum flow that it can take otherwise the water would

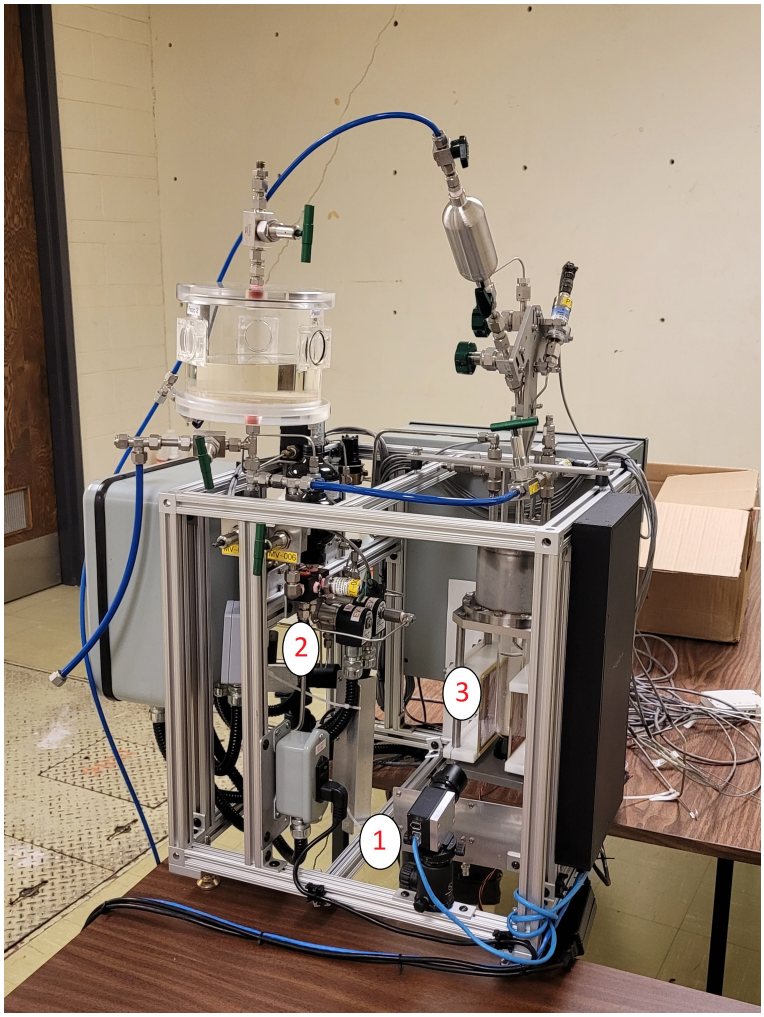

Figure 2.2. Photo of the PICO-0.1 detector. 1: A Basler A602f camera. 2: Hydraulic pressure system. 3: PICO-0.1 inner vessel.

spill out of the bath. The cooling system contains around 19.79 L of water that needs to be cooled by about 3°C starting from ambient temperature. The cooling cycle is slow and cannot be used to rapidly change the temperature of the system and at the same time change the Seitz threshold. Instead, PICO detectors use a pressure system to do so.

The temperature of the water is cooler near the inlet at the bottom of the bath. The difference between the temperature at the bottom of the inner vessel and the top of the inner vessel is less than 0.2°C, the temperature of the jar is assumed to be the same as the temperature measured at the bottom of the bath.

2.2.2. Hydraulic pressure system

The hydraulic pressure system consists of the various valves, pumps and accumulators all filled with mineral oil that controls the pressure of the detector. Figure 2.4 shows the

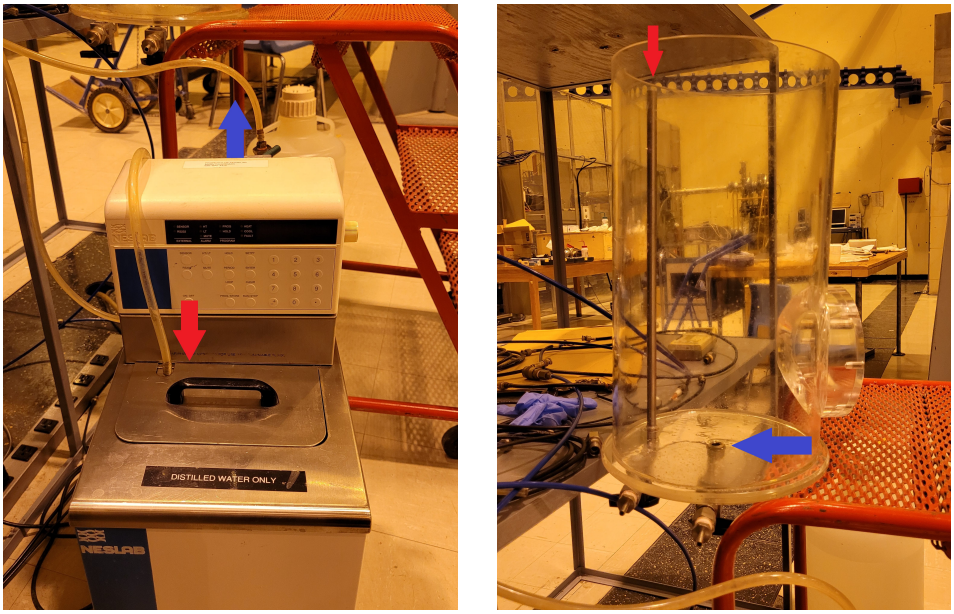

Figure 2.3. Photos of the chiller (on the left) and the water bath (on the right). The water in the chiller is pumped following the tube (blue arrow) and enters the water bath through the bottom (blue arrow). The water circles back to the chiller via an overflow tube in the water bath (red arrow) and enters the chiller via a tube (red arrow)

schematic of the hydraulic system and its different pressure regions. The hydraulic pressure system is not directly connected to the inner vessel to avoid exchanging contaminants. It is separated by two bellows that allow the pressure in the hydraulic system to apply a force on the fluid in the inner vessel, controlling the pressure of the active fluid in the jar.

The hydraulic pressure system uses two accumulators in order to control the pressure during expansion and compression. The accumulator, AC-002, is the low-pressure accumulator. It is regulated by the air regulator that opens when the pressure is above 15 psi. The accumulator, AC-001, is the high-pressure accumulator. They are connected by a pump, PU-001, that will bring mineral oil from AC-002 towards AC-001 setting the pressure at around 210 psi. In the Compress state, the compression valves in the high-pressure side shown in blue, EV-001 and EV-004, are open and the detector is inactive. This means that the perfluorocarbon is in a pure liquid phase and no bubble can form inside the inner vessel. In the Expanded state, the compression valves, EV-001 and EV-004, are closed and the expanding valve on the low pressure side shown in green, EV-005, opens to release some amount of pressure for the inner vessel. The pressure system can control the pressure to a precision of around 0.5 psi. Once the set pressure has been reached, the detector is active and bubbles can be formed following the Seitz model.

Once a bubble has been formed and a camera detects it, it sends a trigger to activate the pump and compress the bellows at pressure between 180 psi and 210 psi. This in turn

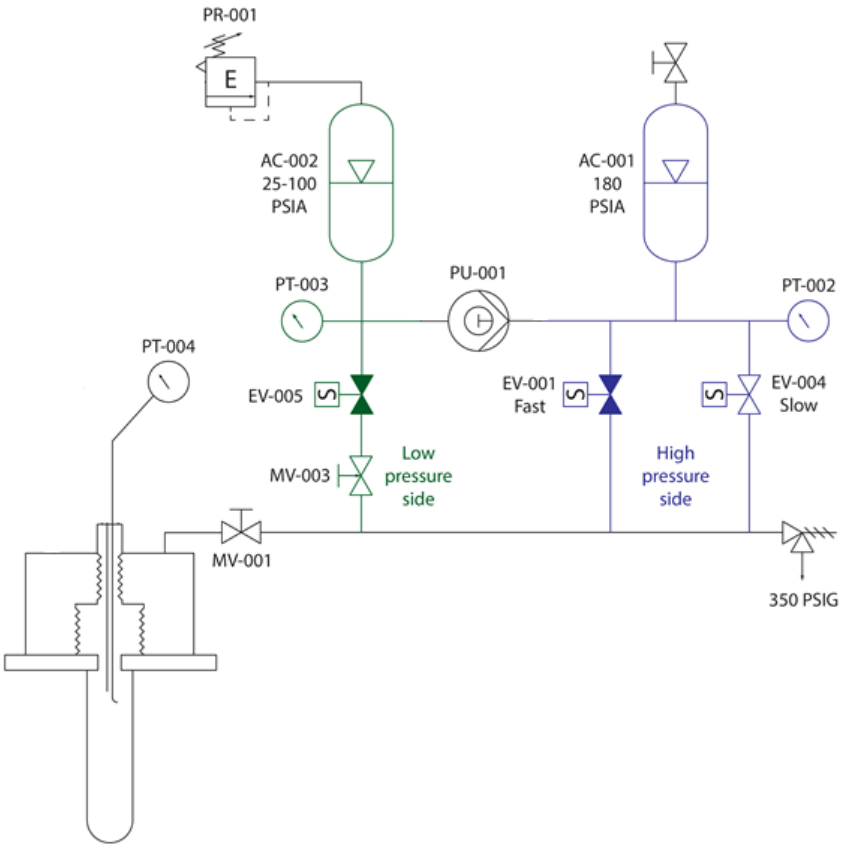

Figure 2.4. Diagram of the pressure system of PICO-0.1. In green is the low pressure region and in blue is the high pressure region of the hydraulic system.

pressurizes the jar and has the bubble collapse. At this point the detector is inactive and no bubble can form. After a few seconds, the system is ready to do another cycle.

2.2.3. Cameras

The bubbles are captured by two Basler A602f cameras running at 120 frames per second. The cameras are positioned at a distance of around 26 cm from the jar, one is positioned behind the jar on the beam line path and the other at 90° angle as can be seen in Figure 2.5. Sixteen LEDs illuminate the jar for the cameras to be able to see it.

The bubbles are detected by comparing consecutive frames. If the intensity of a pixel varies enough between two consecutive frames, the pixel will be flagged as a hitpix. If the number of hitpix is above a certain threshold between two subsequent images, then a trigger will activate the compression system. Otherwise, the number of hitpix is reset. The trigger can be generated by either camera.

While testing the detector in the preparation for the data acquisition, it was noticed that a signal of around 60 Hz was affecting both cameras. This signal due to an unavoidable

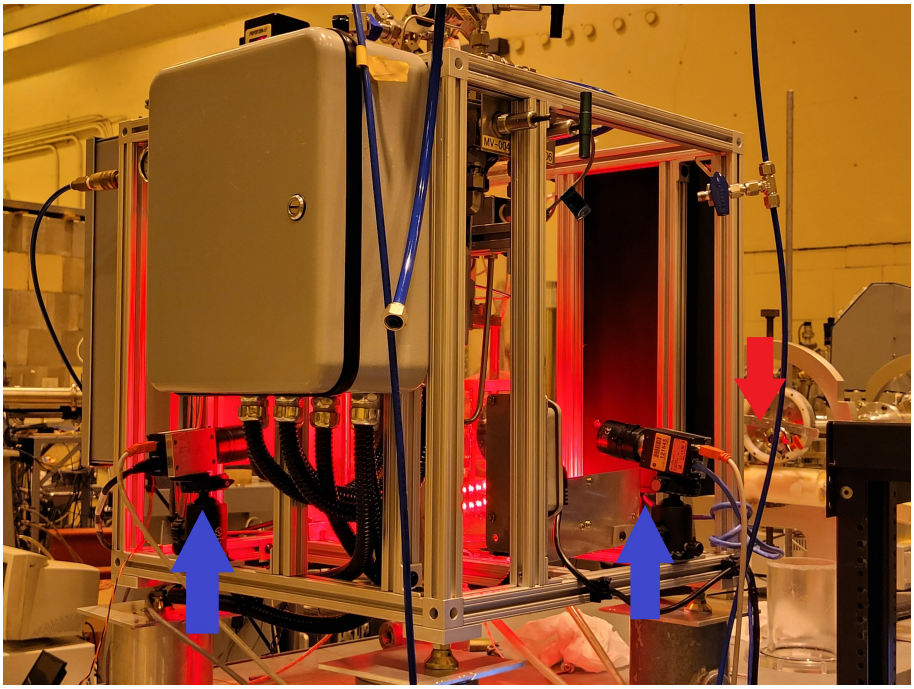

Figure 2.5. Photo of the camera setup. The blue arrows indicate the two cameras and the red arrow indicates the target of the beam.

ground loop, was augmenting the mean intensity of all the pixels for a single frame, causing spurious triggers. To circumvent this issue, the frame rate of the cameras was changed to 120 frames per second and the data acquisition software was modified so that the number of hitpix threshold needed to be met during three consecutive frames to trigger a compression. As bubbles grow in between the frames, this did not affect trigger efficiency. When a bubble is detected, the camera triggers the compression system and registers the last 10 frames on an event.

The PICO collaboration is known for its use of acoustic signals to discriminate between different particles. Piezoelectric sensors were not used in this experiment since the background is significantly lower than the neutrons produced from the vanadium target. It was therefore assumed that every excess event was produced by neutrons.

2.3. Calibration

In order to calibrate the detector, we can use particles that would mimic a theoretical dark matter signal. Neutrons are a good candidate since they are neutral particles and will elastically interact with a nucleus. Mono energetic neutrons between 34 keV and 104 keV were created by the resonant production on vanadium-51.

At those energies, we can approximate the neutron to be non-relativistic. We can derive an equation for the energy recoil of the nucleus depending on the incident neutron shown in eq. 2.3.1,

$$E_r = 2E_n \frac{M_A M_n}{(M_A + M_n)^2}(1 - \cos\theta) \tag{2.3.1}$$

where, E_n is the energy of the neutron, M_A is the mass of the nucleus, M_n is the mass of the neutron and θ is the scattering angle of the neutron. We can calculate the $E_{r,max}$ by imposing $\theta = \pi$ and using the target mass as either a carbon or a fluorine nucleus composing the perfluorocarbon targets (C_3F_8 or C_4F_{10}). The maximum recoil energies as a function of neutron energy are,

$$E_{r,Cmax} = 0.28 \cdot E_n, \tag{2.3.2}$$

$$E_{r,Fmax} = 0.19 \cdot E_n, \tag{2.3.3}$$

If we assume that the neutron elastic scattering is isotropic than the rate of events per recoil energy will have a box shape function for the recoil energy has seen in Figure 2.6. We can see in the same figure that the contribution of the fluorine is bigger than the contribution of the carbon because of the higher number of fluorine atoms in both C_3F_8 and C_4F_{10}. Following the Seitz model, a bubble can only be formed if the recoil energy is higher than a threshold energy. The detector response will be a linear function of to the threshold energy because of the box shape energy and equations 2.3.2 and 2.3.3 seen in Figure 2.6. The total response of the detector will be the sum of the contribution of every atom in both C_3F_8 and C_4F_{10}.

As the scattering is not completely isotropic, due to p-wave scattering, simulations used to calculate the neutron scattering use the r-matrix calculated differential cross sections [21].

The fluid also has a bubble nucleation efficiency; energy deposited above the critical energy will not always form a bubble. The PICO collaboration tried different functions to model it: exponential or error function [19]. It was found that none of those functions could accurately model the efficiency. It was instead proposed to use a 5-point function. In this function, we define 5 efficiency nodes at 0.0, 0.2, 0.5, 0.8 and 1.0. We then assume a linear relation with the recoil energy in between those points. Figure 2.7 shows a fit of this 5-point function at two different thresholds. Each node is fitted by the two recoil species (fluorine and carbon) and by two energy thresholds (2.45 keV and 3.2 keV). The latter two energy thresholds were used because of the extensive data taken by the PICO-60 at those Seitz thresholds. This creates a model with 20 free parameters that we can use to fit the simulation to our experimental data.

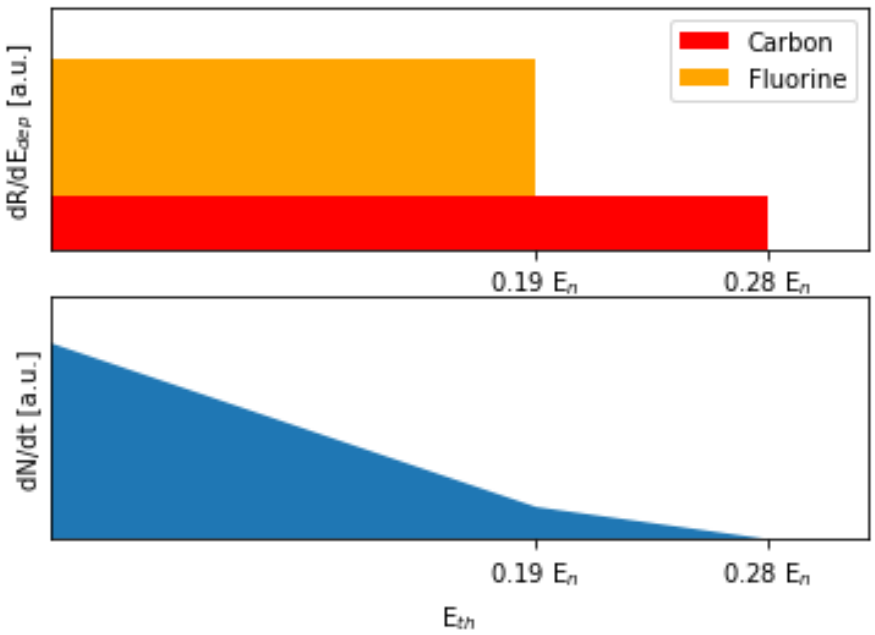

Figure 2.6. Box shape of the recoil spectrum of mono-energetic neutrons. The top figure is the recoil spectrum assuming an isotropic elastic scattering. The bottom figure is the nucleation rate assuming a linear response from the detector.

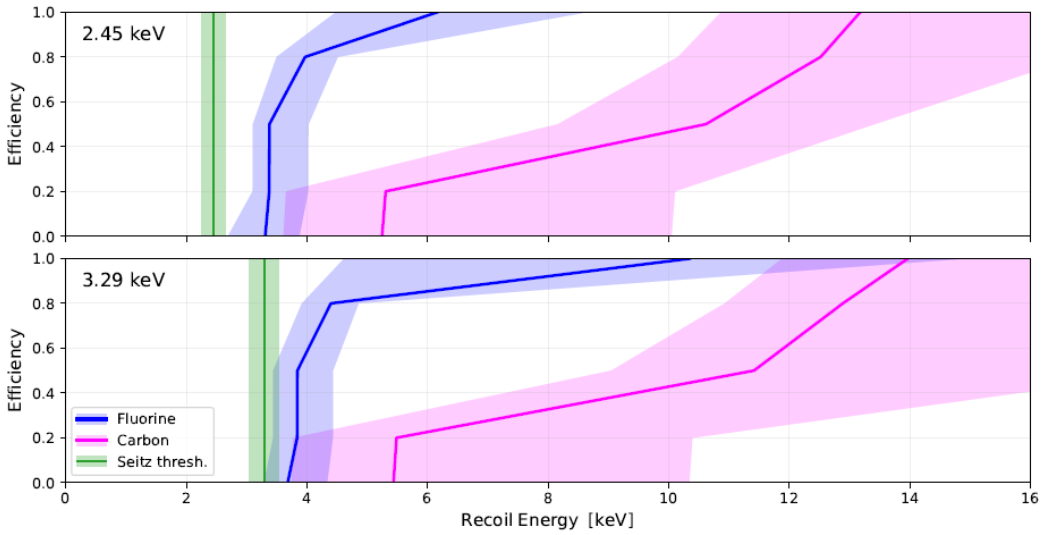

Figure 2.7. Fit of the recoil energy on a fluorine atom (blue) and a carbon atom (pink) compared to the Seitz threshold (green) made using the 5-point function and the PICO-60 detector data with C_3F_8 [22].

The bubble nucleation efficiency of fluorine and carbon recoils are expected to be different because of their charge and mass differences. Fluorine will have a shorter mean range which

implies that more of its energy remains in a critical radius and it should have a higher bubble efficiency than carbon.

For a dark matter interaction, we substitute the energy and mass of the neutron with that of dark matter in equation 2.3.1. With the mass of WIMPs between 2 GeV/c^2 and 100 TeV/c^2 and a constraint on their velocity of $\sim 0.001c$, we would expect to have a maximum nuclear recoil on fluorine of around 0.07 keV to 36.5 keV, depending on the mass of the WIMPs. We would then need neutron energies of around 0.36 keV to 192 keV to simulate similar recoil energy.

2.4. Tandem

The Tandem at the Université de Montréal is an ion pelletron accelerator. It was built in 1966, supervised by René-J. A.-Lévesque and is now in a building that bears his name. The acceleration tube comes from the Chalk River laboratories. The tandem has a terminal voltage of 6 MV and it is the first Tandem accelerator prototype in the world [23]. The Tandem accelerator possesses four important components: the injector, the pelletron acceleration tube, the energy analyzing magnet and the target as can be seen in Figure 2.8.

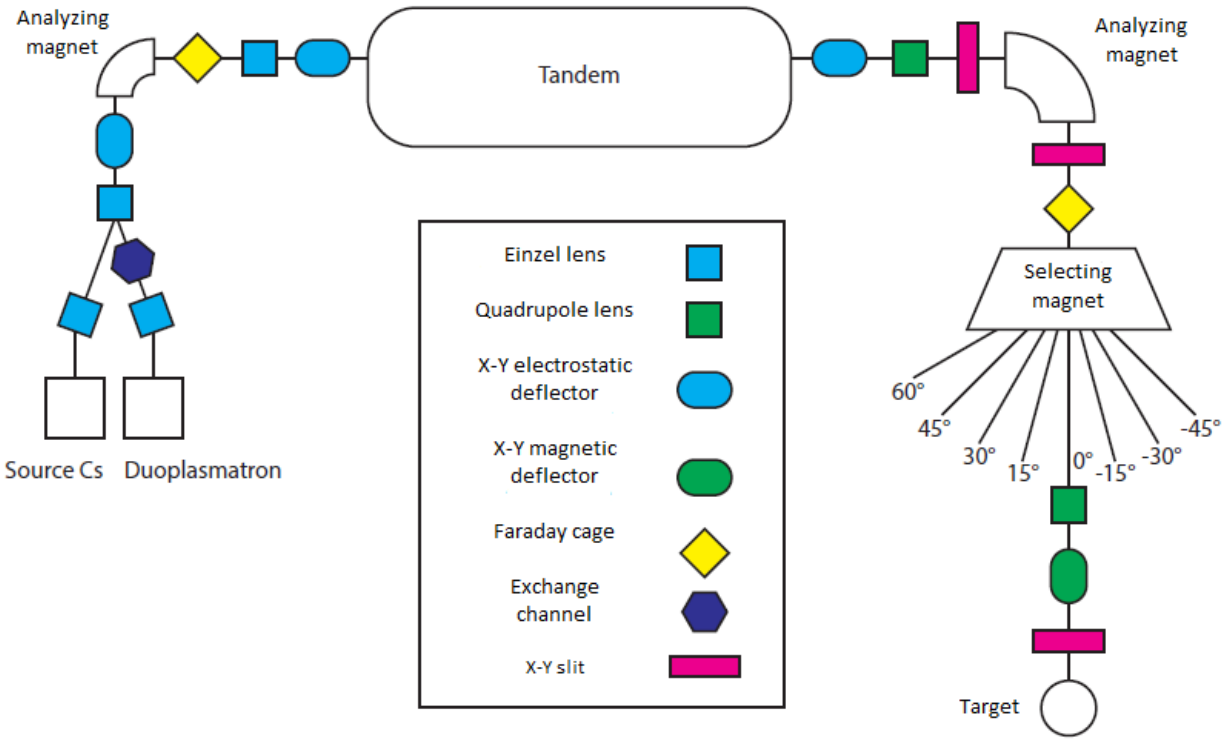

Figure 2.8. Diagram of the Tandem at Université de Montréal [translated from French, 24, fig. 8.9].

2.4.1. Injector

The tandem has two ion sources from HV Engineering Europa: 360 duoplasmotron and 860 sputtering. Those sources create the ion beam that can later be accelerated. The duoplasmotron was used to produce the proton beam. It contains hydrogen gas that can be used to produce a plasma. The duoplasmotron creates this plasma in two steps. First, a coated filament is heated up to eject thermal electrons which will sustain an initial gas discharge of hydrogen into the chamber. Then, the ions are extracted by a strong local magnetic field which produces a high density plasma between the intermediate anode, where the first discharge happens, and the main anode. At the end of the anode is an extraction cone kept at 20 kV. It is placed off-center in order to extract negative hydrogen (H^-), which has two electrons. Those negative ions are focused by Einzel lenses to concentrate the beam towards the first analyzing magnet that deviates it at a 90° angle towards the Q-snout. The magnet will also reduce the energy spread of the beam. If the ion has too high kinetic energy, it won't be deviated enough to stay and if the ion has too low energy, it will be deviated too much to keep in the beam. The ions with the right energies will be able to reach the Q-snout. The Q-snout is used to prepare the beam before entering the pelletron accelerator.

2.4.2. Pelletron accelerator

The Pelletron accelerator is made of a large tube containing stainless steel ring, pelletron chains and an electron stripper. The tube contains multiple stainless steel rings which are used to create an electric field and accelerate the ions. The tube is filled with an SF_6 gas to avoid spark. To produce the high-voltage current, two pelletron chains are used to collect positive charges from an electron gun and transport them towards a terminal at the center of the tube which can withstand a maximum voltage of 6 MV. This voltage is then transferred to the stainless steel ring through a series of resistors of multiple values to ensure a uniform acceleration across the tube which helps avoid sparking. This acceleration is also independent of the radial distribution of the ions.

In the middle of the tube, there is an electron stripper made of a stream of oxygen gas that removes the two electrons from the H^- to obtain positive charged protons. Without the stripper, the negative hydrogen would oscillate from one side of the tube to the other indefinitely. By removing the two electrons, the now-positive hydrogen is accelerated a second time in the other half of the tube. The ions are accelerated twice through the terminal.

2.4.3. Energy analyzing magnet

Not all protons exit the accelerator tube with the same energy. It is necessary to use a second energy analyzing magnet to constraints the proton beam energy to a narrower spectrum. To achieve this, the proton beam is deviated again at a 90° arc and passed through

a slit. The beam becomes nearly monoenergetic since protons with different energies than the one desired would be deviated off of the collider by having either a wider arc for larger energies and smaller arc for lower energies. Those protons would ultimately hit the slit which sends a retroactive loop in the tandem to correct the proton energy and maximize the beam intensity for a given magnetic field. The uncertainty in the proton energy is 0.2 keV for a magnetic field resolution of 0.1 Gauss. For the neutron calibration, the proton energies used were around 1.5 MeV to 1.7 MeV.

After the second energy analyzing magnet, the beam is sent towards the beam selector magnet. This latter magnet is used to deviate the beam in the x- and y-axis (with z being the direction of the beam) into one of seven beamlines where various experiments can take place. The tandem can only supply one beamline at a time. The PICO-0.1 detector was set up on the 0° line. After this selector beam, quadrupole magnet helps focus the beam towards the target of the experiment.

2.4.4. Target

In this experiment a vanadium-51 target was used because of its production of monoenergetic neutrons through the Breit-Wigner resonance of the ^{51}V(p,n)^{51}Cr reaction in the desired range. The target was mounted on a carousel (shown in Figure 2.9) that allows to change the target and conserve the vacuum. Table 2.1 shows the different neutrons energies used and the corresponding peak found by J.H. Gibbons which can be seen in Figure 2.10 [25] as a function of the incoming proton energy.

Proton energy (MeV)	Neutron energy (keV)	Peak
1.592	34	IV
1.607	50	VII
1.629	74	IX
1.651	97	XI
1.658	104	XII

Table 2.1. Identified peaks of resonant production of neutron on a ^{51}V [25].

We measure the neutron flux production at each energy. The neutron energy is not completely monoenergetic since there is a certain width of the resonances for the various peaks coming from the elastic recoil of protons unto the nuclei of the target. In those collisions, the electrons will collect a part of that recoil inducing some uncertainty in the neutron kinetic energy of the same order as the uncertainty from the energy analyzing magnet.

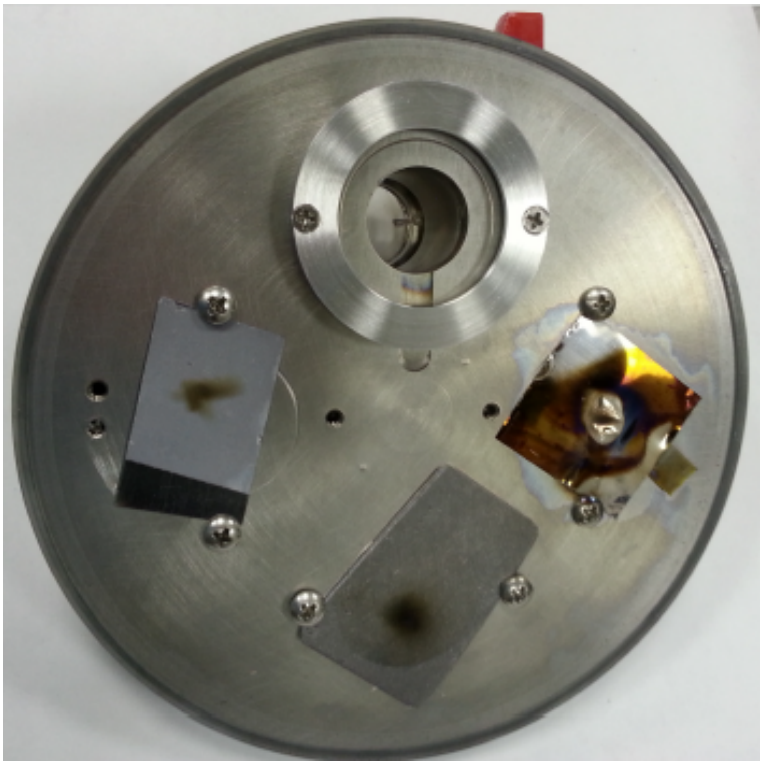

Figure 2.9. Photo of the carousel with various targets: vanadium, lithium and tantalum [24].

The cooling bath used water to shield the perfluorocarbons from thermal neutrons. A beam tube was added to the bath to avoid neutron scattering of the neutron beam. The neutron propagation was simulated by Alan Robinson with a detailed geometry of the detector set up of both PICO-0.1 and the He3 proportional chamber.

Since the carbon and fluorine nucleus have neutron elastic scattering resonances with neutron interaction close to the ^{51}V resonances, we need to take into account the neutron-carbon and neutron-fluorine cross section presented in Figure 2.11.

2.5. Mixing procedure

In previous experiments with PICO detectors, pure perfluorocarbon was used. In this thesis, we used a mixture of C_3F_8 and C_4F_{10}. Multiple techniques can be used to create a fixed mix of both perfluorocarbons like pre-mixing before the fill. To avoid mass partitioning in the filling line of the C_3F_8 and C_4F_{10}, it was decided to directly mix the perfluorocarbons inside the PICO-0.1 jar. The full step-by-step procedure can be found in the appendix A. The perfluorocarbon masses are presented in table 2.2.

The PICO-0.1 detector is a right side down detector, meaning that the jar opening is pointing upwards. If any perfluorocarbon gas were to go upwards and lodged itself in the bellows, it could cause a problem in the compression cycle of the detector. The detector would

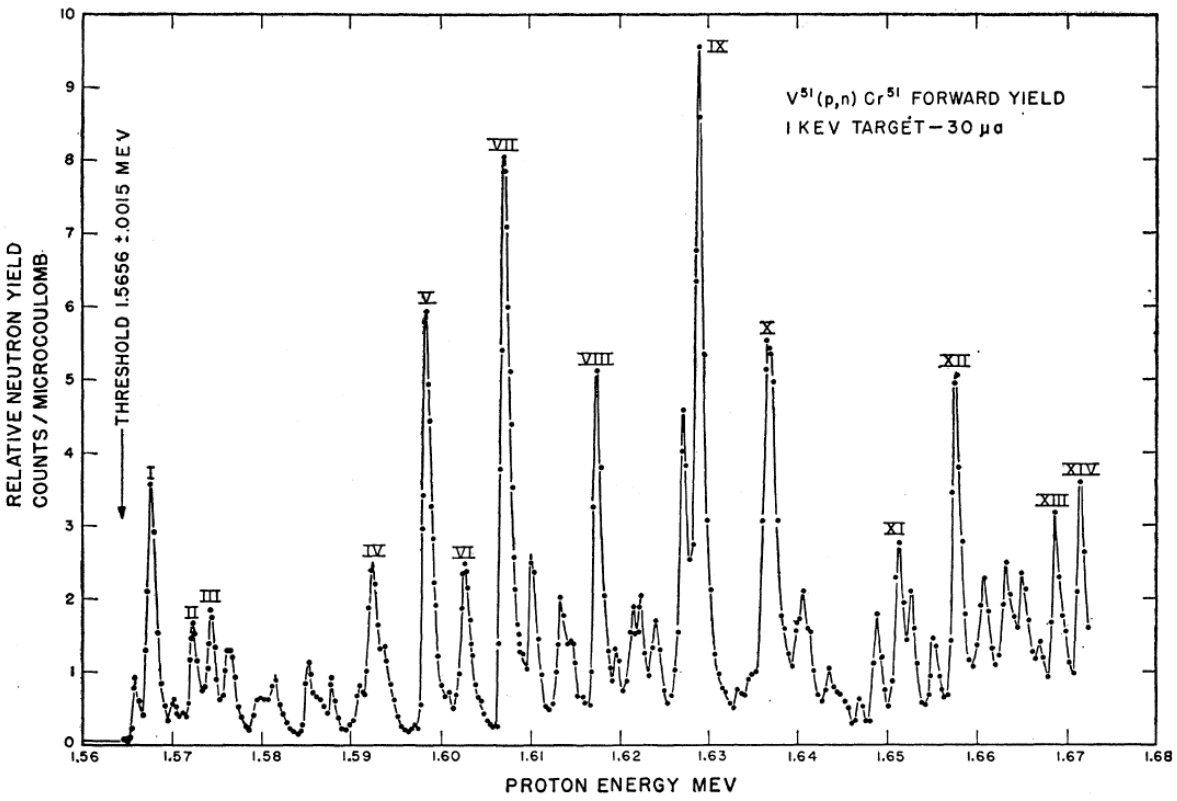

Figure 2.10. ^{51}V(p,n)^{51}Cr resonance as function of the incoming proton energy [25].

fail to return to an active volume and it could boil during expansion. In order to avoid this issue, the jar was first completely filled with degassed LAB (*Linear Alkyl Benzene*) completely isolated and under pressure. Since both liquid perfluorocarbons have a higher density than the LAB the perfluorocarbon droplets would fall down. To condense the perfluorocarbon, the water bath surrounding was cooled down to $\sim$3°C before opening the valve and letting the perfluorocarbon in through the middle valve in Figure 2.12. The flow was regulated in order for the perfluorocarbon to have enough time to condense. Since the jar is completely isolated apart from the perfluorocarbon inlet, the droplets cannot enter because of the fixed volume filled with incompressible fluid. It was then necessary to partially open the jar to air in order for some LAB to come out (through the left valve in Figure 2.12) and make room for the perfluorocarbon droplets.

The first perfluorocarbon filled was the C_4F_{10} because it has a higher boiling point. If the C_3F_8 was filled first, its higher vapour pressure would have prevented the C_4F_{10} from entering the chamber. To measure the amount of each perfluorocarbon and therefore their ratio, the bottle containing each perfluorocarbon was weighted. During the fill, the mass of the bottle was also measured to have a sense of the amount of perfluorocarbon dropped inside the jar. After the fill, the bottle was cooled down in order for the perfluorocarbon gas

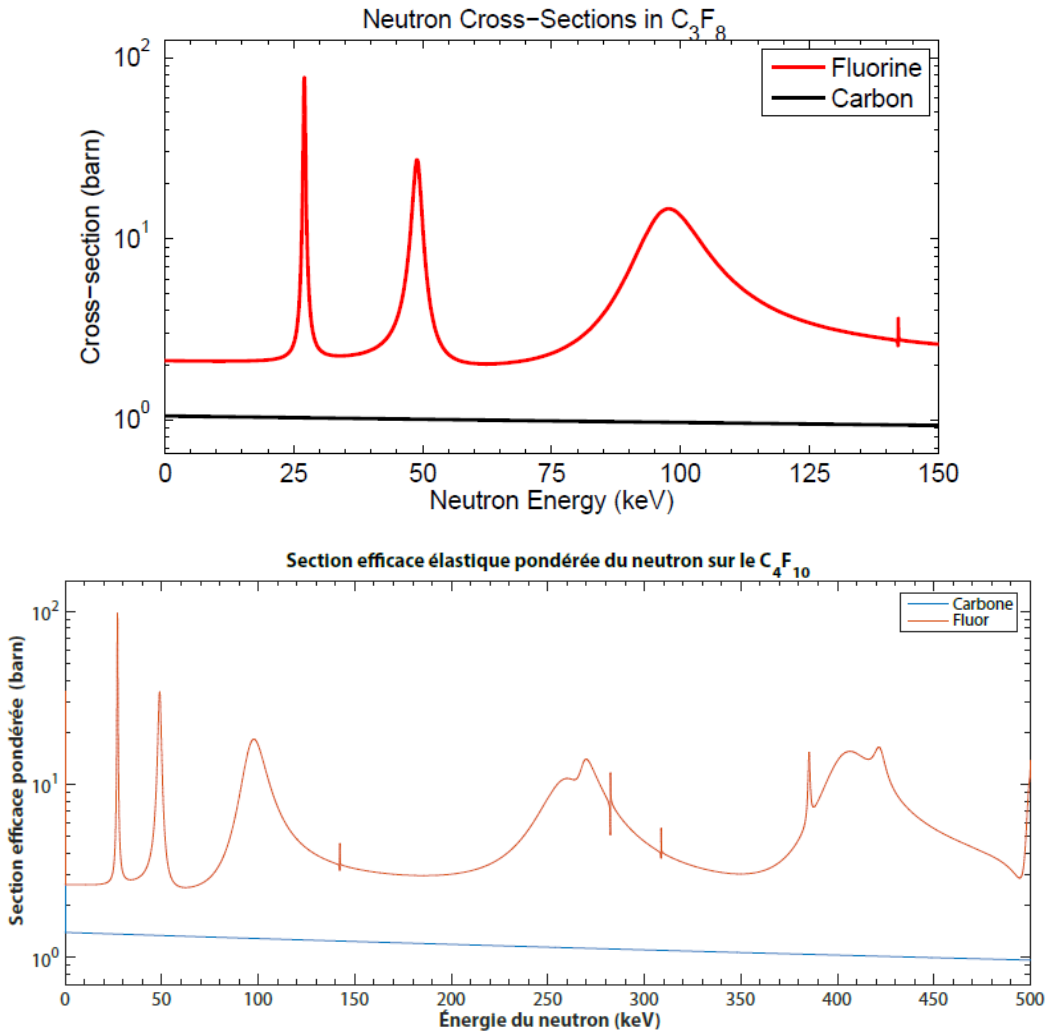

Figure 2.11. Neutron-fluorine and neutron-carbon cross section weighted for C_3F_8 on top [26] and for C_4F_{10} below [24] as a function of neutron energy.

inside the connecting tube to condense back into the bottle. The bottles were again weighted to have an accurate measurement of the total perfluorocarbon used.

This procedure has the advantage of accurately measuring the total perfluorocarbon after the fill is completed. It is, however, incapable of accurately measuring it during the fill making it difficult to set a particular ratio. This procedure has the obvious disadvantage of being very sensitive to small error. The flow of the perfluorocarbon entering the jar is dependent on the pressure inside the jar, but the act of pushing perfluorocarbon inside has in itself an impact on the pressure. If the perfluorocarbon doesn't completely condense before entering the jar, it can cause an issue with the compression. Lastly, if after the fill, the perfluorocarbon doesn't fully condense back into the bottle then the mass measured will lose in accuracy. For the last possible issue, we can know that it fully condenses back into the bottle if we have trouble pulling the connecting tube out since it was initially in a vacuum.

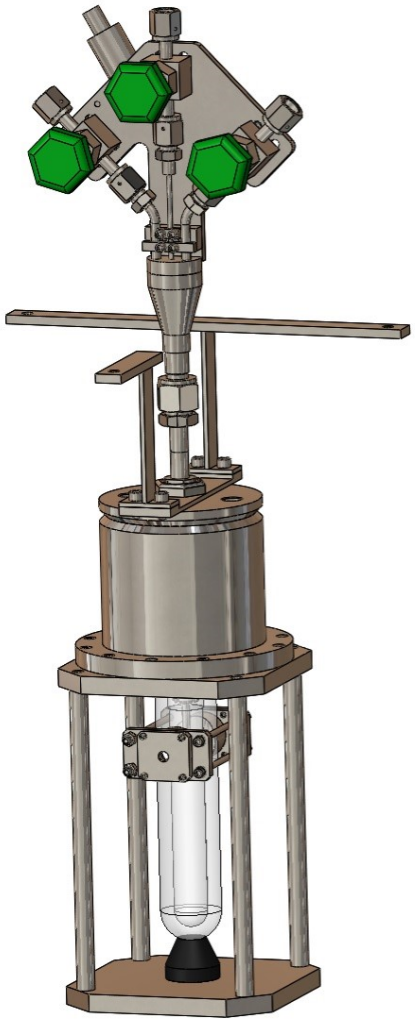

Figure 2.12. Design of PICO-0.1 and the valves used for the mixing procedure, made by Mathieu Laurin SVG: A-01-A01-A - Detector.

Perfluorocarbon	Mass (g)	Volume (mL)
C_3F_8	66.41 ± 0.01	95.63 ± 0.01
C_4F_{10}	11.67 ± 0.01	18.44 ± 0.01

Table 2.2. Mass of the perfluorocarbons used.

Chapter 3

Data and Analysis

In this chapter, the data and its acquisition setups will be presented. Data acquisition was made of background sources to take them into account. The detector stability and data cuts will be presented. Finally, the analysis will be presented. In the analysis, we can expect to see an explanation of the bubble multiplicity identifying algorithm that I made specifically for this work and a simulation of the expected nuclear recoil distribution was made by Alan Robinson. The consistency of the event rates were double checked using the absolute neutron rates emitted by the vanadium-51 target.

3.1. Data

The data were taken using two detector setup. The main part was taken using the PICO-0.1 detector to acquire the data necessary to calibrate the perfluorocarbon mixture. In the second part, an absolute neutron flux measurement was made using two He-3 proportional chambers. Background measurements were made of both setups. Finally data temperature and pressure stability measurements were done in order to choose quality cuts to be made.

3.1.1. PICO-0.1 data

PICO-0.1 data were taken during two periods: the first one between November 2021 and December 2021 and the second one between February 2022 and March 2022. The periods will be later described as the 2021 data/periods and the 2022 data/periods respectively. In both runs, the temperature was set at 17.5°C and the pressure for an event was set to randomly alternate between a pressure of 30 psi, 49.44 psi and 53.5 psi between each event. A description of data from these periods is given in table 3.1 with details described below. The neutron energies used were previously given in table 2.1. For the 34 keV and 50 keV neutrons, only the 30 psi pressure was used as the maximum energy deposition would have been similar to the theoretical bubble nucleation threshold and the expected number of events would be

comparable to the background. Table 3.1 presents the daily data acquisition, the neutron energies used and some additional details concerning the run.

Day	Neutron energy (keV)	Details
2021-10-27	97	
2021-11-05	97	Inability to obtain 30 psi
2021-11-09	74	
2021-11-10	74	
2021-11-11	74	
2021-11-12	50, background	
2021-11-13	background	
2021-11-14	background	
2021-11-15	background	
2021-11-16	background	
2021-11-17	background	
2021-11-18	background	
2021-11-19	background	Tandem broke
2022-02-14	74, 97, background	Only 30 psi data
2022-02-15	50, 74, background	Only 30 psi data
2022-02-16	background	Only 30 psi data
2022-02-17	background	Only 30 psi data
2022-02-18	background	Only 30 psi data
2022-02-19	background	Only 30 psi data
2022-02-28	34, 50	Only 30 psi data
2022-03-01	34	Only 30 psi data
2022-03-03	104, background	
2022-03-04	104, background	
2022-03-05	background	
2022-03-06	background	
2022-03-07	background	PICO-0.1 broke

Table 3.1. Daily data acquisition and neutron energy for the PICO-0.1 detector.

Early in the 2021 runs, it was noticed that the inner vessel pressure was not able to reach the set pressure of 30 psi. This issue only happened for this set pressure. It was found that the valve (MV-003 in Figure 2.4) was tightened to a point where the hydraulic system couldn't release its pressure in the required time allowed by the control system. The issue

was fixed when the valve was opened. The 2021 runs ended because of a mechanical issue with the tandem which took nearly 2 months to fix. At the beginning of the 2022 runs, it was decided that we would focus on retaking the 30 psi data before using new neutron energies.

It was intended to take data using a LiF target with a neutron energy of around 150 keV. However, an issue with the PICO-0.1 hydraulic pump made it impossible to continue the data acquisition. It was decided that the repair would be delayed awaiting results from another PICO-related project.

Table 3.2 presents the expected bubble nucleation threshold from the Seitz model hot spike and at the equilibrium of mass transport. In the hot spike regime, the bubble forms faster than the rate of transport of molecules from the gas region into the interface in-between the gas and liquid and the transport of the molecules from the interface towards the liquid region. This creates a discontinuity of the chemical potential at the interface between the gas an liquid region. At the equilibrium of mass transport, the bubble forms more slowly allowing the molecules to travel through the gas into the interface at the same rate as the molecules travelling from the interface towards the liquid phase. This allows the chemical potential to be equal on both sides of the interface and effectively reduces the required energy for bubble nucleation.

Pressure (psi)	E_{Seitz} [keV] (hot spike)	E_{Seitz} [keV] (at equilibrium of mass transport)
30	3.6	3.0
49.44	10.2	8.3
53.5	13.6	10.6

Table 3.2. Theoretical Seitz thresholds of the hot spike and of the equilibrium of mass transport for the set pressure and the perfluorocarbon used in the PICO-0.1 data.

Table 3.3 presents the different run conditions for every neutron energy, E_n at each pressure. We can also see the total live time, bubble multiplicity events (1, 2, 3+), number of neutron measured by the He-3 source and the total current measured.

3.1.2. Neutron flux

In order to measure the neutron flux emitted from the vanadium-51, two He-3 proportional chambers were used. The first one was placed underneath the target during all the data taking and the second one was suspended at approximately the position previously occupied by the jar of PICO-0.1. These He-3 counters will be referred to as He-3 source and He-3 hanging respectively. The He-3 source was also present during the PICO-0.1 data

E_n (keV)	Pressure (psi)	Live time (s)	Events (1, 2, 3+)	He-3 counts	Charge (a.u.)
34	30	27163.24	(193, 9, 2)	273	24783
50	30	16169.76	(478, 54, 3)	1102	58608
74	30	8245.29	(410, 32, 3)	1018	50197
	49.44	14360.49	(230, 3, 3)	2546	29512
	53.5	14389.24	(86, 6, 0)	2772	11883
97	30	6402.24	(359, 67, 7)	293	49123
	49.44	4215.49	(171, 8, 0)	251	22915
	53.5	4629.78	(125, 1, 0)	386	14948
104	30	6213.98	(197, 28, 7)	220	26348
	49.44	5927.04	(150, 15, 2)	212	21025
	53.5	4801.67	(137, 13, 4)	147	20233

Table 3.3. Run conditions for the neutron energies and the pressures used in the PICO-0.1 data.

acquisition in order to monitor the neutron flux during all the data taking. The data with the second He-3 counter and PICO-0.1 removed was taken between May 2022 and July 2022. The He-3 source was in a moderator of paraffin wax and the He-3 hanging was in a moderator of ultra-high-molecular-weight polyethylene of known composition and shape as an absolute neutron flux calibration. The He-3 source had a custom preamplifier combined with a single-channel analyzer (SCA) that automatically filtered background noise. The signal was then sent to a counter. The He-3 hanging was connected to an Ortec 142PC preamplifier, a separate SCA and a counter. Calibration of this SCA was made using a multi-channel analyzer and an Ac-Be neutron source.

Day	Neutron energy (keV)
2022-05-13	34, background
2022-06-03	50, background
2022-06-08	74
2022-07-26	34, 74, background
2022-07-27	97, background
2022-07-28	34, 104

Table 3.4. Daily data acquisition and neutron energy for the neutron flux measurements.

3.1.3. Background

Both PICO-0.1 and the He-3 counters are sensitive to environmental neutrons and internal α particles. The water bath was used to shield against environmental neutrons and a beam tube was added for the neutrons emitted from the vanadium-51. Both the environmental neutron rate and the internal α particle rate were measured together. In other PICO detectors, α contamination is a big source of background. This contamination can come from the trapping of radon gas or impure material with thorium or uranium chains. This background is less important for this work because of its low event rate, compared to the event rate of the beam. To mitigate the α background, PICO-0.1 was disassembled and cleaned using Radiacwash to reduce radon contamination. The detector was then reassembled in a clean room.

3.1.4. Detector temperature and pressure stability

The stability of the detector ensures that the Seitz threshold for bubble nucleation remains constant. Figure 3.1 shows the pressure of the inner vessel for every event. The data was separated into the 2021 data and the 2022 data. At first, we can notice the relative instability of the early events of the 2021 data which was fixed when the valve MV-003 was adjusted. We can see that a major part of the 2022 runs were set at 30 psi since most of the 30-psi runs made in 2021 did not achieve the set pressure as can be seen by the absence of data in the 30-psi line. This is because the detector failed to reach within 1 psi of the set pressure in the allocated time. Figures 3.2 and 3.3 respectively show histograms of the pressure of the inner vessel and temperature T1 of each beam time event weighted by the total live time of the event. In the pressure histogram, we can observe a peak at each of the set pressure (30, 49.44 and 53.5). We can also observe that the pressure system is stable to around 0.5 psi considering the width of the peaks. In the temperature histogram, the vast majority of the events are contained in an interval of 0.25 °C with a mean of 17.6 °C.

PICO-0.1 has three temperature sensors labeled T1, T2 and T4. The number of the temperature sensor is in order of height meaning T1 is the lowest point closest to the water inlet and T4 is the furthest which is closer to the water outlet. The inner vessel is positioned at a height between T1 and T2 with T1 being closest to the inner vessel. All further reference to the inner vessel temperature will refer to the T1 temperature. Figure 3.4 shows the temperature at various points in the bath at each event. At first, we can notice a difference in the temperature of T4 between the 2021 data and 2022. This is because the valve controlling the inlet flow of the water was adjusted to cycle the water at a faster rate. Some of the instability in the water temperature can be explained by a low water level in the chiller causing the water to cycle at a slower rate. The step in the 2022 data can be explained

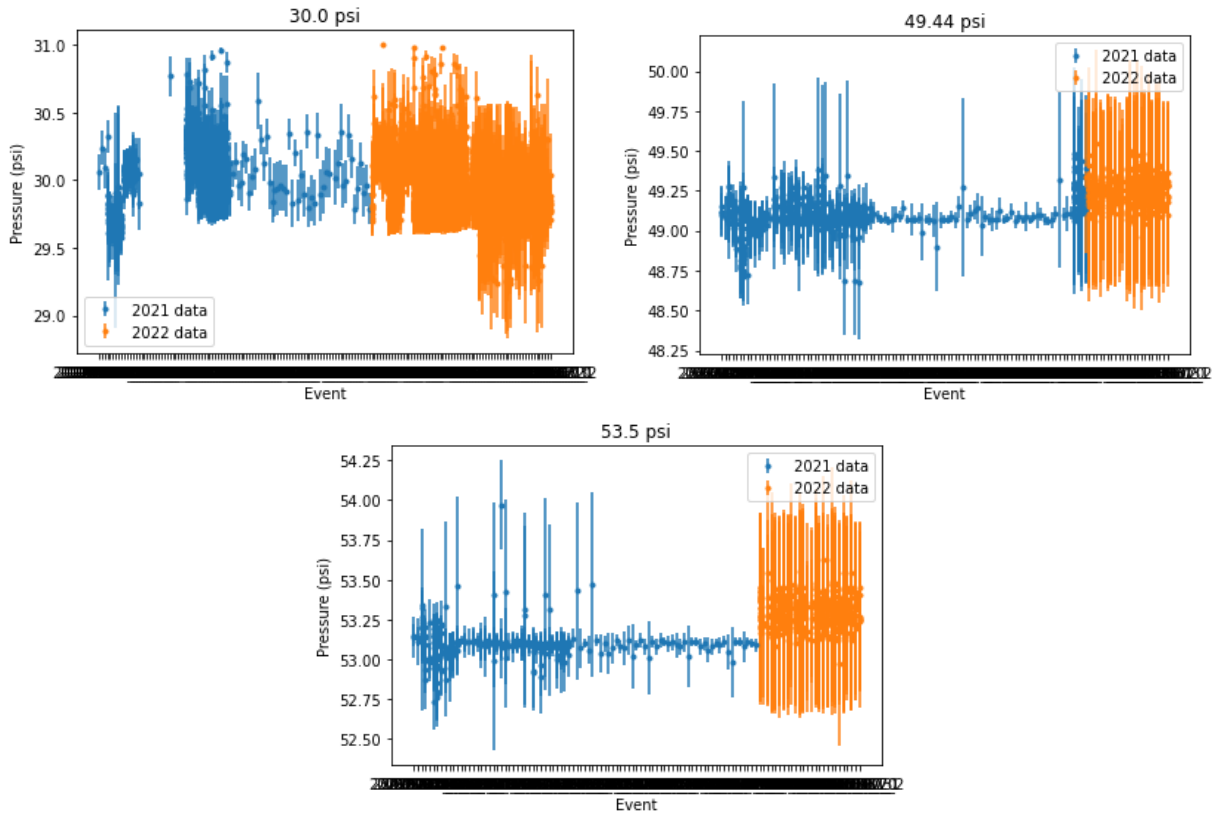

Figure 3.1. Inner vessel pressure separated into the 2021 data and 2022 data for each set pressure.

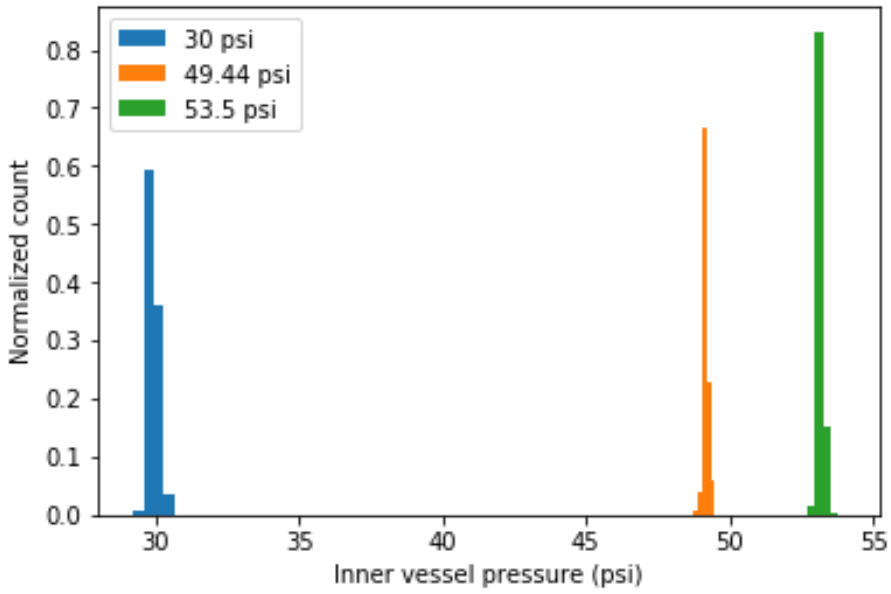

Figure 3.2. Histogram of the inner vessel pressure during beam data weighted by live time.

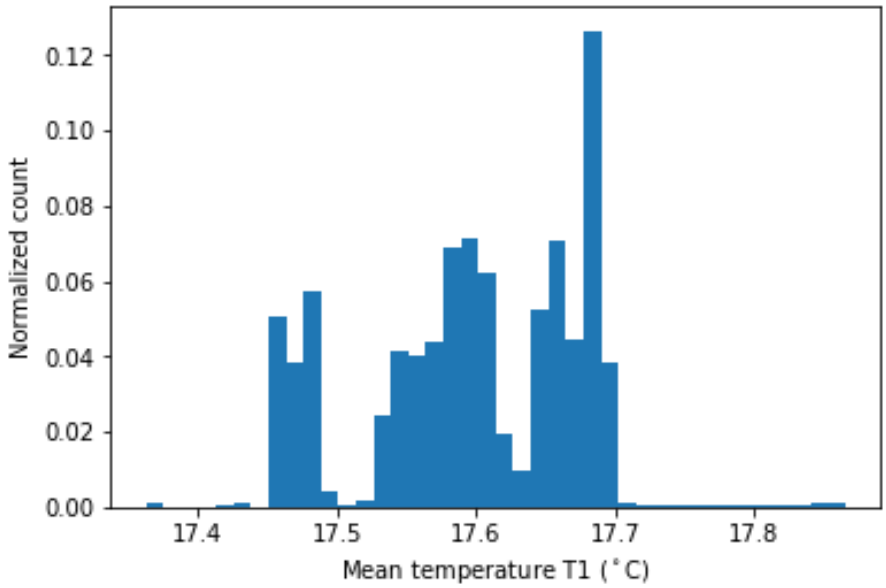

Figure 3.3. Histogram of the temperature T1 weighted by live time.

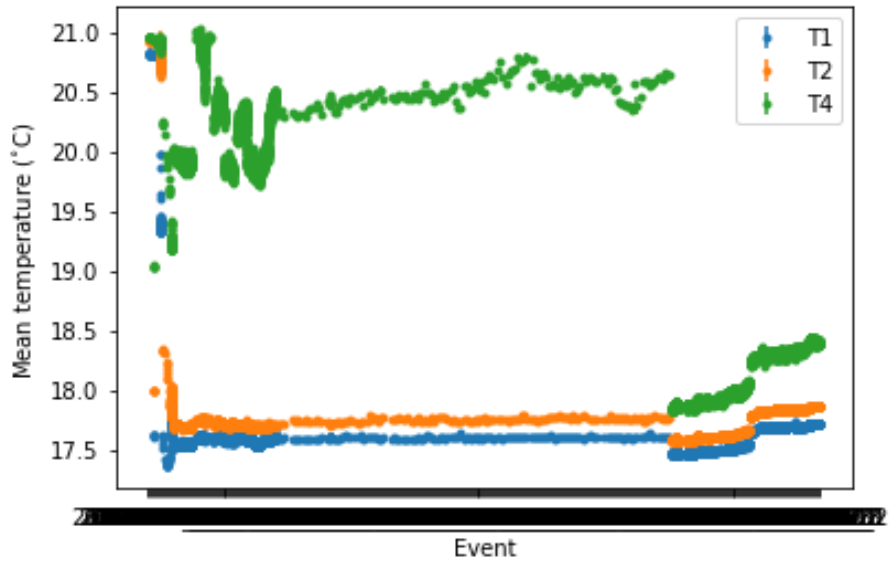

Figure 3.4. Temperature of the water bath at every event separated into the 2021 data and 2022 data.

by a change in the chiller set temperature to 17.3°C to compensate for the apparent offset in the T1 temperature due to the increased inlet flow.

3.1.5. Data quality cuts

Following the stability analysis, data cuts were made for data quality assurances and data were grouped in order to calculate a common threshold value. No acoustic cut was

made since there was no acoustic sensor used in this work. A pressure cut was applied to remove event where the pressure inside the inner vessel was within 0.5 psi of the set pressure in order to ensure that the desired threshold was obtained. For the 30 psi set pressure, this cut was at 1 psi within the set pressure. A temperature cut was applied for temperature (T1) above 18°C. The interval of pressure was within 0.2°C of the set temperature, 17.5°C. This removed the early events where the chiller was not properly running. The data were grouped into three Seitz thresholds, one for each set pressure: 3.6 keV (30 psi), 10.0 keV (49.44 psi) and 13.3 keV (53.5 psi).

3.2. Analysis

In the data analysis, I created an algorithm to find discriminate between events with zero bubble and events with a single bubble. A geometric simulation of the detector setup for both data acquisition (PICO-0.1 and neutron flux) based on previous calibrations [27] was adapted to the new detector position. From the simulation results, a maximum likelihood estimation was made to find the expected Seitz thresholds for the three set pressures.

3.2.1. Bubble multiplicity

In order to identify the number of bubbles in an event, the PICO collaboration has developed an algorithm called Autobub [28]. It uses the entropy from each camera angles to determine the number of bubbles and their position in the image. However, during our experiment, one of our cameras was partially blocked by a recently installed copper mesh intended for future tests of the detector as can be seen in Figure 3.5. The Autobub algorithm could not work properly. For this reason, I developed a prototype algorithm to reduce the number of events that would need to be manually scanned. Since Autobub was not working properly, it was not possible to do a 3D reconstruction of the event and discriminate the bubbles forming on the surface of the jar.

The idea behind the prototype algorithm is similar to how the cameras detect a bubble in the first place: by looking at the intensity variation. It works by calculating the average and the variance of the intensity of every pixel across the 10 frames of an event. The average over the 10 images should effectively remove the bubble and the variance should instead show only the bubble as can be seen in Figure 3.6 a)-b). A threshold is then applied to the variance image so that only the pixels where the intensity varies enough (i.e. when there is a bubble) are flagged. This third image is called the hitpix image seen in 3.6 c). It was noticed that events without bubble had very few flagged pixels. There is a condition that if the number of flagged pixels is too low, the event is considered a zero bubble event.

If the previous condition is met, the algorithm then determines the center of the bubble by calculating the average position of the flagged pixel weighted by the variance of the

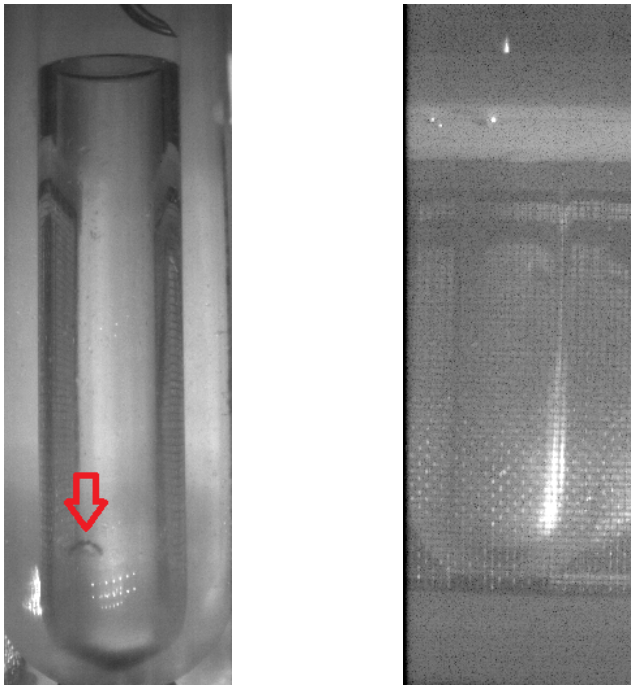

Figure 3.5. Images from both camera angles with a bubble visible on the left camera, but not in the right camera 1.

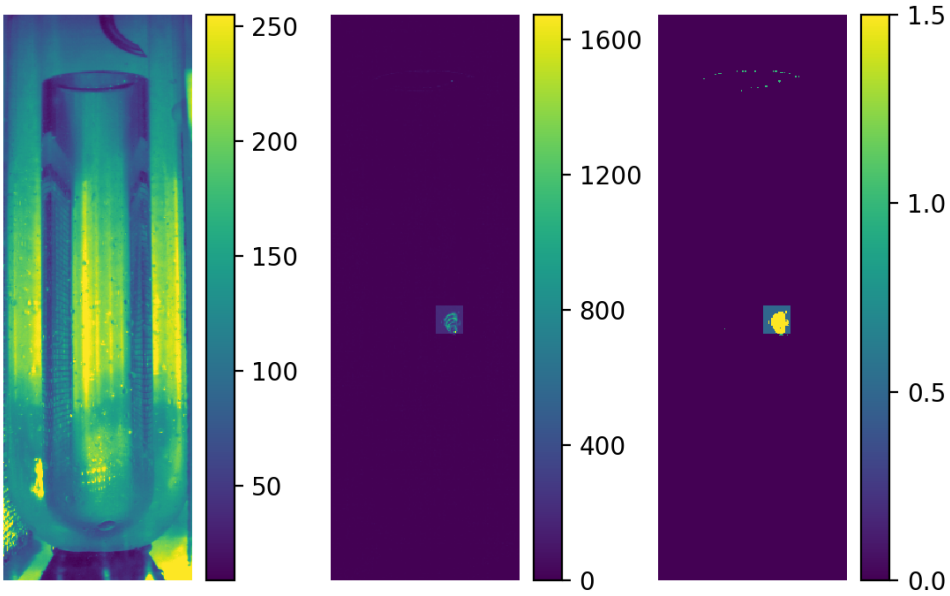

Figure 3.6. Images of the mean pixel intensity (left), the pixel intensity variance (center) and the hitpix (right).

intensity. It is possible that some random pixel will vary enough to be flagged, especially

considering the 120 Hz signal previously observed. Those random flags tend to have a lower variance than the flagged pixel from an actual bubble. Once the center of the bubble has been determined, there is a condition that rejects events that are too close to the surface between the perfluorocarbon and the LAB. The algorithm creates a square of side r_1 (instead of a circle for simplicity of coding) around the center of the bubble. It is then measured the ratio of the number of flagged pixels inside the square on the number of flagged pixels in total.

$$pixel\ containment\ ratio = \frac{\#\ of\ \ flagged\ pixels\ inside\ the\ square}{\#\ of\ \ flagged\ pixels\ in\ total} \tag{3.2.1}$$

If the pixel containment ratio is above 0.97, then it passes the first test, otherwise it is considered as an event to be manually reviewed. This condition is followed by an almost identical condition, but the square has a side r_2, where $r_1 > r_2$ and a much higher threshold for a flagged pixel. The idea behind this condition is to discriminate between single bubble event and 2+ bubbles event. The center of the bubble has a much higher variance than the edge because the bubble expands across the various frames. If the center calculated is not at the center of a bubble, it is very much likely that the second square will not contain the entire bubble which will be the case for 2+ events. If the event fails this condition, it is flagged for manual review. After the manual scan, the bubble multiplicity was categorized into 3 groups: single bubble events, two bubble events and 3+ bubble events. The last category was made inclusive due to the low number of events with three bubbles or more.

The algorithm was tested on a sample of 984 events that were manually scanned. It was able to successfully identify every faulty event (e.g. events where the LEDs are not turned on). It was capable of having an identification rate of 56.1% over the total amounts of event with an error rate of 1.1% of the events being incorrectly labelled. The algorithm was then applied to the full data set. The identification rate dropped to 38.8%. It is possible that the significant drop in identification rate is due to differences in the camera aperture and LED intensity in between the different measurements.

The accuracy of the algorithm was not further pushed since the goal was mainly to reduce the number of events that needed to be manually scanned. OpenCV is a Python image processing package and many of its modules could be used to further developed this prototype. It is unlikely that it will be needed since the present algorithm is used only in the limited case of the PICO-0.1 detector.

3.2.2. Simulation

Simulations provide an expected number and energy of nuclear recoils against which I am calibrating PICO-0.1. The neutron flux simulation was done using MCNPX-Polimi [29]. The simulation calculated the path and scattering of neutrons from the vanadium-51 target

to various objects in the detector setup. It also calculated the amount of energy deposited at each interaction site. The simulation recreated some key elements of the geometry of the whole detector assembly including its support as can be seen in Figures 3.7 and 3.8. Simulations were made for all neutron energies with both the PICO-0.1 setup and the absolute neutron flux setup.

In Figure 3.7, we can see in the simulation picture the beam line in gray and to the right, we see the water bath with its beam tube. Inside the bath is the PICO-0.1 inner vessel and the hydraulic system on top of it. The supports and instruments have also been accounted for in the geometry. The black moderator seen in the SolidWorks image was removed from the simulation geometry as it was not present during the data acquisition. In Figure 3.8, we can observe in the simulation picture, again, the beam line to the left and suspended to the right are a moderator, which contains a He-3 counter and on top of it is its preamplifier. In the real photo, we can see the two He-3 counters in red, the preamplifier in blue and the beam line in green. The distances and size of the water bath, the suspended He-3 counter was updated to reflected changes to their position. The distance between the vanadium-51 target and the jar was measured with an uncertainty of 2 mm. Most of this comes from the uncertainty of the compression in the copper mesh which hindered our ability to accurately measure the distance. The total volume of the perfluorocarbon fill is 53.5 $\pm$ 0.5 mL. The uncertainty comes in part from the measurement but also from the uncertainty in the amount of perfluorocarbon gas stuck in the fill line.

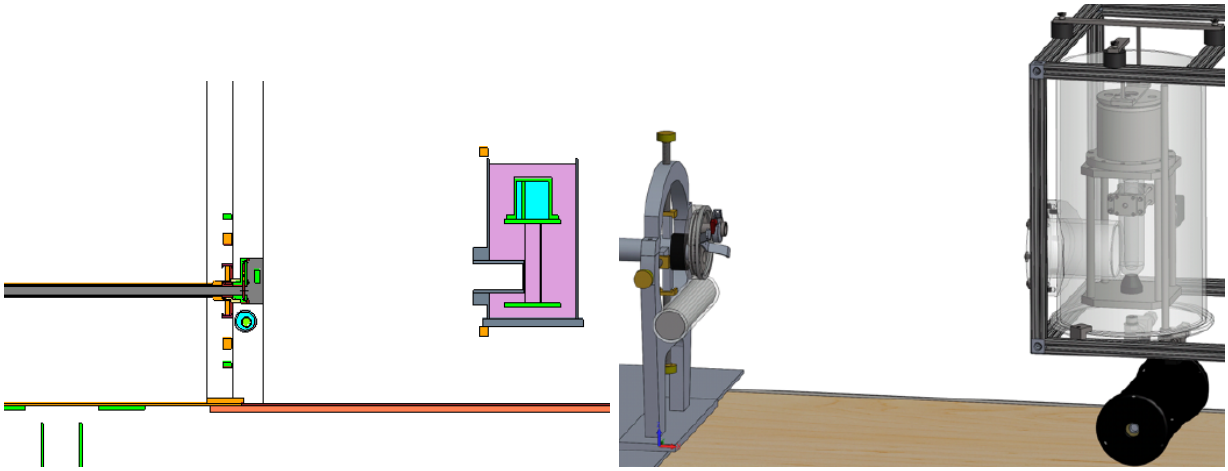

Figure 3.7. Image of a slice seen from the side of the simulated PICO-0.1 detector (left) compared to a SolidWorks photo (right)[22]. See text for a detailed description.

Using the energy deposition of neutrons in the mixture, we were able to determine the proportion of neutrons which would have deposited enough energy to produce a bubble event. The efficiency parameters determined by the PICO2L runs (Figure 2.7) allowed us to find the proportion of neutrons that produced one bubble, two bubbles and three or more

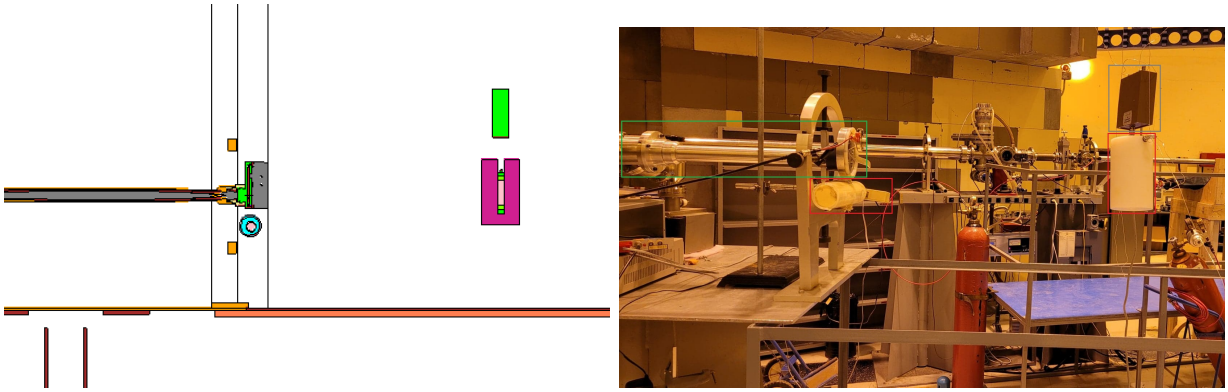

Figure 3.8. Image of a slice seen from the side of the simulated He-3 counter (left) compared to a real setup (right). See text for a detailed description.

bubbles. These efficiency parameters were only used in the 30 psi case because it is expected that the bubble nucleation efficiency would follow a similar curve for similar threshold (3.6 keV expected for the mixture and 3.29 keV for the PICO2L runs). For the higher pressure, it would be expected that the bubble nucleation efficiency would look like a step function. Therefore, the step function was used for the probability function at 49.44 psi and 53.5 psi.

The simulation results also allows us to obtain an absolute bubble rate. Considering the uncertainty in the normalization of this rate from both helium-3 measurements and the geometrical uncertainty, it is more fruitful to use the ratio of the bubble multiplicity to fit the Seitz threshold. Given our high statistics, the measured single bubble event rate provides our normalization. In the exhaustive analyses [30, 31] of the pure C_3F_8 bubble nucleation efficiency, the ratio of bubble multiplicity provided the greatest weight in their fits.

Chapter 4

Results

In this chapter, the results will be presented in detail. The measured neutron flux ratio will be compared to the simulation. The bubble multiplicity rate will be presented along with the expected rate calculated from simulations. This will lead us to obtain the energy calibration and compare it to the theoretical values. Finally, we will be able to answer our initial questions concerning the future use of PICO-500.

4.1. Neutron flux

The neutron flux emitted by the vanadium-51 was measured in order to convert the number of neutrons depositing enough energy to produce a bubble to the number of bubbles measured. Table 4.1 presents the ratio of simulated and measured neutron detection between the He-3 source detector over the He-3 hanging detector. We can see a similar value between the simulated ratio at each neutron energy. Similarly the measured ratio is similar at each neutron energy. However, when comparing the simulated and measured ratio, we observe significant differences. These differences can be explained by the fact that the calibration of the He-3 source is not precisely known, thus why the measured ratio is used to calibrate it. We suppose that the discrepancy is due to uncertainty in the efficiency of the He-3 source detector. More analysis will be done to try to identify the cause of that discrepancy.

4.2. Bubble multiplicity

The bubble multiplicity rates were calculated in order to see the consistency of the data and as a way to find the expected energy threshold as will be shown in section 4.3.1. Figure 4.1 shows the rate of bubble multiplicities at different pressures and neutron energies. The rates were normalized by the single bubble events of the same energy and pressure. We can see in the figure that in higher pressures, the rate of two bubbles events and 3+ bubbles events tends to decrease and with almost no 3+ bubbles events at 53.5 psi. There are multiple uncertainties relating to the bubble rates. We have the background which happens

Neutron energy (keV)	Simulated Ratio	Measured Ratio
34	10.53	3.71 ± 0.18
50	8.4	5.0 ± 0.2
74	9.31	4.16 ± 0.18
97	8.63	3.56 ± 0.17
104	7.2	4.5 ± 0.2

Table 4.1. Measured and simulated ratio of the total neutron detected in the He-3 hanging over the total neutron detected in the He-3 source for each neutron energies. Only the statistical uncertainty is presented.

randomly in time and another relating to the number of neutrons emitted. We also have an uncertainty of 3% in the neutron-fluorine interaction cross section, or equivalently its mean free path, that will dominate most of our results. This uncertainty adds up for every bubble (3% at 2 bubbles, 6% at 3 bubble, 9% at 4 bubbles, etc.). Lower thresholds increase the rate of multiple bubble events compared to single bubble events for a given neutron energy.

4.3. Simulations

The simulations are a crucial part of the analysis. In order to find the energy threshold, it is necessary to use simulations to compare previous calibrations to the current one. To achieve this, we are simulating the expected number of neutrons that will deposit enough energy to produce a bubble for a given threshold. We call them the bubble multiplicity vectors. The probability for a given number of bubbles per neutron trajectory is calculated by modeling a Bernoulli process with non-identical probabilities defined by the efficiency function used. The probability vectors for each neutron trajectory are summed across all simulated neutrons to obtain an expected event rate per emitted neutron. Table 4.2 shows the bubble multiplicity vectors found using this method for every neutron energy and set pressure used.

4.3.1. Energy calibration

To account for non-linearity in the effect of Seitz threshold on event rates (eq. 1.2.5), a maximum likelihood estimation was used in order to find this threshold for every set pressure using all the neutron energies and the bubble multiplicity. Using a set neutron energy and a set bubble multiplicity, we can suppose that the statistical distribution is going to be following a Poisson distribution (eq. 4.3.1), where n is the bubble multiplicity and μ is the number of measured bubbles multiplied by the simulated ratio of bubble multiplicity over the single bubble event.

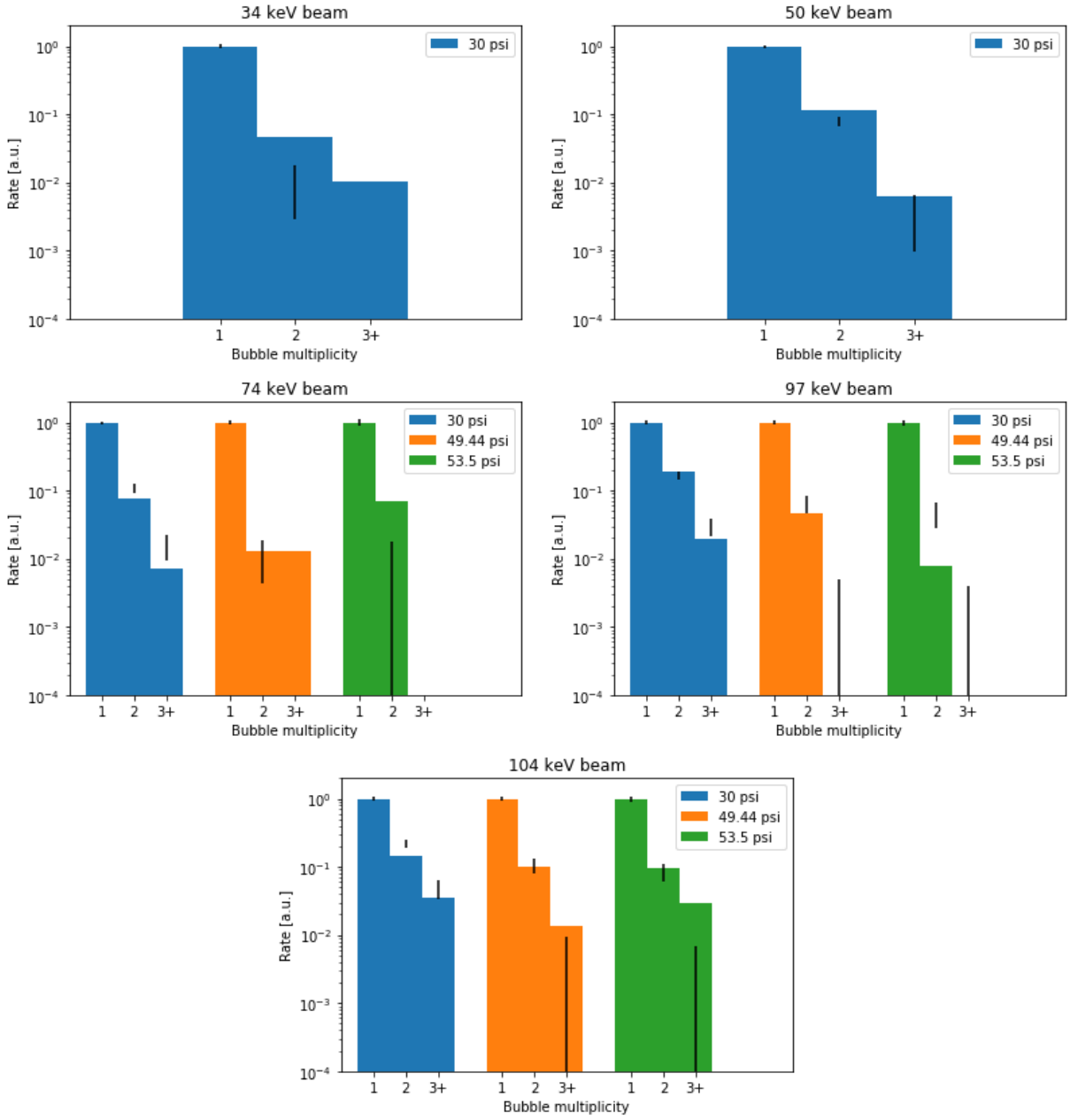

Figure 4.1. Normalized measured rate (bars) and expected rate (error bars) of bubble multiplicities for different set pressures and beam energy. Poisson statistical uncertainties are shown on the best fit expected rates.

$$P(X = n) = \frac{\mu^n e^{-\mu}}{n!} \tag{4.3.1}$$

To find the likelihood function, L, we need to multiply all these probabilities together (eq. 4.3.2), where i is every combination of the five neutron energies with each of the two bubble multiplicities (2, 3+) divided by the single bubble events for a total of 10 combinations.

Neutron energy (keV)	Pressure (psi)	1 bubble	2 bubbles	3+ bubbes
34	30	10400	366	2.013
50	30	43800	4260	358
74	30	3560	4540	782
	49.44	16300	684	12.0
	53.5	6160	63.0	0.0
97	30	69400	12800	2690
	49.44	56600	6940	617
	53.5	47300	2810	72
104	30	66100	16000	4090
	49.44	53400	8810	1010
	53.5	46000	4460	167

Table 4.2. Expected number of bubbles per 7×10^8 neutrons emitted from the vanadium-51 target at a given neutron energy and assuming the efficiency curve shown in 2.7 at 30 psi and a step function at 49.44 psi and 53.5 psi.

$$L = \prod_{i=1}^{10} \text{Pois}(\mu_i) \tag{4.3.2}$$

Using the natural logarithm of the likelihood function and assuming a normal distribution for the bubble nucleation threshold, we can find the maximum likelihood which will give us the expected threshold. We can find the standard deviation, s, using equation 4.3.3,

$$\ln L = \ln L_{max} - s^2/2. \tag{4.3.3}$$

From the plots of Figure 4.2, we can find the expected threshold for each pressure by looking at the minimum of the curve, which corresponds to the maximum likelihood. Table 4.3 presents the theoretical thresholds in the case of a hot spike, in the case of mass transport equilibrium and as measured for each set pressure used. The 30-psi data strongly favours the hot spike model.

At the higher pressure, the step function Seitz threshold is displaced from the expected onset of detector efficiency, as expected, by several keV. In contrast, the efficiency function at 30 psi as measured in C_3F_8 accounts for energy lost in bubble nucleation of $\sim$1.5 keV. However, at both higher pressures the data is consistent with the Seitz model plus a similar energy loss.

We can conclude that in the case of a C_3F_8 and C_4F_{10} mixture, we are not in the mass transport regime. The uncertainty on the measured threshold is determined from the uncertainty of 0.5 psi of the pressure sensor and the uncertainty between the RTD value and the actual inner vessel temperature which is estimated at 0.2 °C.

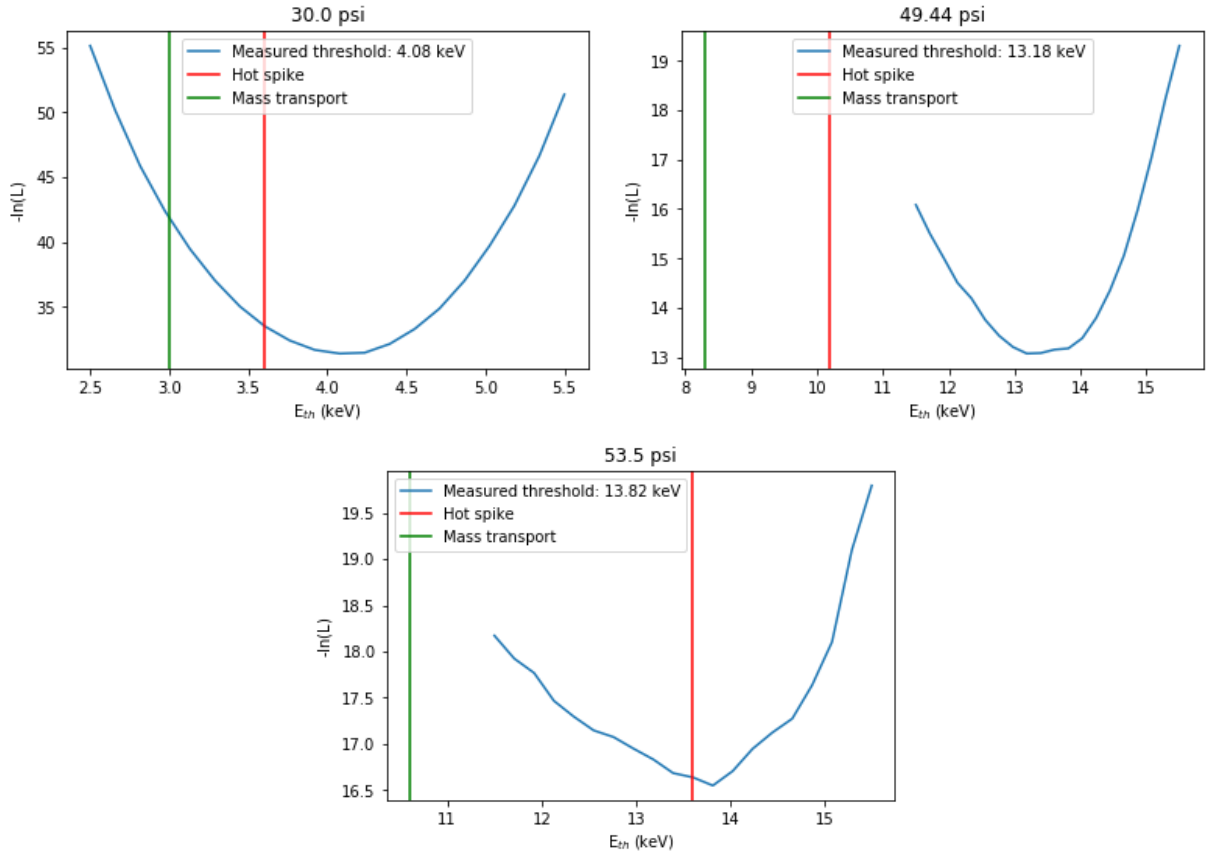

Figure 4.2. Logarithm of the likelihood function of the threshold energy assuming the efficiency curve shown in 2.7 at 30 psi and a step function at 49.44 psi and 53.5 psi.

Pressure (psi)	Seitz threshold [keV] (hot spike)	Seitz threshold [keV] (mass transport equilibrium)	Measured threshold (keV)
30	3.6 ± 0.1	3.0 ± 0.1	4.08 ± 0.19
49.44	10.2 ± 0.4	8.3 ± 0.3	13.2 ± 0.4
53.5	13.6 ± 0.6	10.6 ± 0.4	13.8 ± 1.1

Table 4.3. Theoretical threshold of the hot spike, at equilibrium of mass transport and measured for each set pressure used. Uncertainties in temperature (0.2°C) and pressure (0.5 psi) are propagated in the theoretical Seitz thresholds.

The results at 30 psi are a faithful calibration of this mixture considering the similarity of the threshold with the PICO-2L threshold which used a pure fluid of C_3F_8. It shows that PICO-500 will be able to operate using a 3-4 keV threshold. The results also show that it will be able to operate PICO-500 at higher thresholds in order to avoid to be sensitive to solar neutrinos.

Conclusion

In conclusion, we presented the importance of dark matter search in the understanding of cosmological phenomena, presented an overview of the most popular dark matter models and some experiments search for this mysterious particle. A detailed explanation of the Seitz model which lays the foundation for the use of bubble chambers was presented with limitation on mixture. Bubble chambers were detailed and how small chambers can be used for calibration with the help of an ion accelerator. A detailed description of the data acquisition was shown and the data quality cuts used. A prototype algorithm was able to help in calculating the bubble multiplicity of every event. The simulations of the detectors geometry allowed us to calculate the expected bubble multiplicity rate. By using previous calibration of PICO detectors, we were able to find the energy threshold.

I conclude that PICO-500 will be able to operate using a perfluorocarbon mixture since the bubble nucleation physics is well understood. PICO-500 will be able to operate at a Seitz threshold of 10 keV, as I tested at 49.44 psi, with sensitivity to nuclear recoils starting around 13 keV in order to avoid sensitivity to solar neutrinos. Further analysis will be conducted to find the bubble nucleation efficiency curve of this mixture which was beyond the initial scope of this project.

References

[1] F. Zwicky, "Spectral displacement of extra galactic nebulae", *Helv. Phys. Acta*, vol. 6, pp. 110–127, 1933.

[2] V. Rubin and K. Ford, "Rotation of the andromeda nebula from a spectroscopic survey of emission regions.", *The Astrophysical Journal*, vol. 159, pp. 379–403, 1970.

[3] K. Freese, "Review of Observational Evidence for Dark Matter in the Universe and in upcoming searches for Dark Stars", *EAS Publications Series*, vol. 36, pp. 113–126, 2009. DOI: 10.1051/eas/0936016. [Online]. Available: http://dx.doi.org/10.1051/eas/0936016.

[4] NASA, *NED results for object Bullet Cluster*, Last accessed on 13 January 2022.

[5] NASA/CXC/CfA/M.Markevitch *et al.*, "NASA Finds Direct Proof of Dark Matter", X-ray.

[6] NASA/STScI;ESO WFI;Magellan/U.Arizona/D.Clowe *et al.*, "NASA Finds Direct Proof of Dark Matter", Optical.

[7] D. Eisenstein *et al.*, "Detection of the Baryon Acoustic Peak in the Large-Scale Correlation Function of SDSS Luminous Red Galaxies", *The Astrophysical Journal*, vol. 633, no. 2, pp. 560–574, Nov. 2005. DOI: 10.1086/466512. [Online]. Available: http://dx.doi.org/10.1086/466512.

[8] T. Tait, "Searches for Particle Dark Matter", University of California, Apr. 2014.

[9] L. Roszkowski, E. Sessolo, and S. Trojanowski, "WIMP dark matter candidates and searches—current status and future prospects", *Reports on Progress in Physics*, vol. 81, no. 6, p. 066 201, May 2018. DOI: 10.1088/1361-6633/aab913. [Online]. Available: http://dx.doi.org/10.1088/1361-6633/aab913.

[10] A. Canepa, "Searches for supersymmetry at the Large Hadron Collider", *Reviews in Physics*, 2019. DOI: 10.1016/j.revip.2019.100033.

[11] S. Giagu, "WIMP dark matter searches with the ATLAS detector at the LHC", *Frontiers in Physics*, vol. 7, May 2019. DOI: 10.3389/fphy.2019.00075.

[12] M. SREDNICKI, "AXIONS: PAST, PRESENT, AND FUTURE", *Continuous Advances in QCD 2002*, Dec. 2002. DOI: 10.1142/9789812776310_0032. [Online]. Available: http://dx.doi.org/10.1142/9789812776310_0032.

[13] P. Sikivie, D. Tanner, and K. van Bibber, "Resonantly Enhanced Axion-Photon Regeneration", *Physical Review Letters*, vol. 98, no. 17, Apr. 2007. DOI: 10.1103/physrevlett.98.172002. [Online]. Available: http://dx.doi.org/10.1103/PhysRevLett.98.172002.

[14] F. Seitz, "On the Theory of the Bubble Chamber", *The Physics of Fluids*, 1958. DOI: 10.1063/1.1724333.

[15] T. Kozynets, S. Fallows, and C. Krauss, "Modeling emission of acoustic energy during bubble expansion in PICO bubble chambers", *Phys. Rev. D*, vol. 100, p. 052 001, 5 Sep. 2019. DOI: 10.1103/PhysRevD.100.052001. [Online]. Available: https://link.aps.org/doi/10.1103/PhysRevD.100.052001.

[16] A. Robinson, "Seitz Model for mixtures", PICO Experiment, 2020.

[17] A. Plante, F. Tardif, and V. Zacek, "Understanding the Response to 17 keV ^{35}S-Recoils in C_2ClF_5", PICO Experiment, Feb. 2017.

[18] S. Chen, "Test et calibrations technologiques avec PICO-0.1 pour les futurs détecteurs de chambre à bulle de matière sombre de PICO", M.S. thesis, Université de Montréal, 2020.

[19] F. Tardif, "Direct detection of dark matter with the PICO Experiment and the PICO-0.1 calibration chamber", M.S. thesis, Université de Montréal, 2018.

[20] ChemistNate, *Phase Diagrams*. [Online]. Available: https://www.chemistnate.com/phase-diagrams.html.

[21] A. E. Robinson, "New libraries for simulating neutron scattering in dark matter detector calibrations", *Phys. Rev. C*, vol. 89, p. 032 801, 3 Mar. 2014. DOI: 10.1103/PhysRevC.89.032801. [Online]. Available: https://link.aps.org/doi/10.1103/PhysRevC.89.032801.

[22] B. Ali *et al.*, "Determining the bubble nucleation efficiency of low-energy nuclear recoils in superheated C_3F_8 dark matter detectors", 2022. DOI: 10.48550/ARXIV.2205.05771.

[23] CCPAC, *Installation du CCPAC*. [Online]. Available: https://ion.lps.umontreal.ca/facilities-fr.html.

[24] M. Laurin, "Recherche de la matière sombre à l'aide de détecteurs à liquides surchauffés dans le cadre de l'expérience PICO/Picasso", Ph.D. dissertation, Université de Montréal, 2016.

[25] J. H. Gibbons, R. L. Macklin, and H. W. Schmitt, "V^{51}(p,n)Cr^{51} Reaction as a 5- to 120-kev Neutron Source", 1955. DOI: 10.1103/PhysRev.100.167.

[26] F. Girard, "Calibration of the PICO-0.1 bubble chamber and Development of coated inner vessels for dark matter search", M.S. thesis, Laurentian University, 2017.

[27] A. Robinson, "Dark Matter Limits from a 2L C_3F_8 Filled Bubble Chamber", Ph.D. dissertation, University of Chicago, 2015.

[28] P. Mitra, "PICO-60: A Dark Matter Search Experiment with C_3F_8 in a Bubble Chamber", Ph.D. dissertation, University of Alberta, 2018.

[29] E. Padovani, S. Pozzi, S. Clarke, and E.C.Miller, *MCNPX-PoliMi User's Manual*, 2012.

[30] M. Piro and D. Durnford, "Nuclear Recoil Efficiency Analysis Status", PICO Experiment, Mar. 2021.

[31] M. Jin, "Measurements and Analysis of the Sensitivity of Superheated C3F8 Bubble Chambers to Interactions from WIMP Dark Matter", Ph.D. dissertation, Northwestern University, 2019.

Appendix A

Mixing procedure

This is the procedure to fill the PICO-0.1 detector with a mixture of perfluorocarbon. Figure 2.4 shows the pressure system of the PICO-0.1 detector with the various valves noted as MV-0XX.

A.1. Preliminaries

Install the water bath and cool the water at 3°C. The detector needs to be in compressed and MV-001 closed. PT5 should be at between 180 to 210 psi at this moment.

A.2. LAB fill procedure

The goal of this procedure is to completely fill the jar with LAB in preparation for the perfluorocarbon fill procedure.

1- Connect a fill hose to MV-012 (compression fitting);

2- Open valves MV-010 and MV-011;

3- Pour in LAB from the valve MV-012 until trickles out MV-010;

4- Close MV-010;

5- Continue pouring until it trickles out of MV-011;

6- Close MV-011.

A.3. Hydraulic fill procedure

1- Hook up an oil pump to a high point in the system (preferably the oil reservoir), with a fluid trap in the line;

2- Pump out all air in the hydraulic system ensuring the valves are opened to avoid any trapped air;

3- Close the valve to the vacuum pump;

4- Siphon oil to fill the hydraulic volume from a bucket;

5- Leak open the vacuum line until no air space is left (possibly by using a closed section of hose containing a limited vacuum volume);

6- Isolate the chamber from the hydraulic cart by closing MV-001;

7- Charge the accumulators (AC-001 and AC-002) following the oil refill procedure;

8- Place the hydraulic cart in a compressed state (between 180 and 210 psi).

A.4. C_4F_{10} fill procedure

C_4F_{10} needs to be filled first because of its ebullition point being higher than that of the C_3F_8 so it won't boil during the C_3F_8 fill procedure. The perfluorocarbon needs to condense into liquid to drop at the bottom so it must not be filled to quickly otherwise gas perfluorocarbon will leak upwards and could lodged in the bellows.

1- Ensure MV-001, MV-010, MV-011, MV-012 and MV-016 are closed;

2- Measure and record the mass of the C_4F_{10} source bottle prior to the fill. Leave the bottle on the scale;

3- Connect a fill line with a single vacuum line port to MV-011 and the source bottle;

4- Connect the fill line to the scroll pump and evacuate the line;

5- Close the valve to the vacuum pump;

6- Open the valve to the source bottle;

7- Very gently open MV-011 while monitoring PT4 and the pressure differential (i.e. Pdiff = PT5-PT4). If the pressure differential changes suddenly, close MV-011 and wait for it to stabilize;

8- Continue opening the valve until it is fully opened and droplets start falling;

9- Very slowly partially open MV-010 and leak out LAB into a beaker. As LAB leaks out, C_4F_{10} will fill into the chamber. The speed at which LAB leaks out determines the speed of C_4F_{10} falling in. It is important to look at the pressure diffential since it will also influence the speed of the fill. It is better to have no more than 1-2 droplets falling each second;

10- Continue filling with C_4F_{10} until the scale approximately measures a difference in mass a little under what is desired, then close MV-010. Some C_4F_{10} will still fill for a moment;

11- Place the source bottle into the freezer. The source bottle must still be opened so the gas perfluorocarbon in the line can condense back in the bottle;

12- Wait at least 45 minutes before closing the source bottle;

13- Disconnect the line from the source bottle. It should have a small resistance from the vacuum;

14- Remeasure the mass of the source bottle and calculate the amount of C_4F_{10} filled.

If the procedure needs to be stopped at any point, close MV-010 and MV-011. Out the hydraulic cart under compression and open MV-001. To restart, close MV-001 and continue at step 7.

A.5. C_3F_8 fill procedure

1- Repeat the steps from the C_4F_{10} fill procedure but with the C_3F_8;

2- Once the fill of C_3F_8 is completed, connect the grenade filled with LAB to MV-011;

3- Reconnect the fill line (C_3F_8) to the gas side of the grenade;

4- Push LAB through the fill line leaking it out of MV-010 using the gas pressure from the C_3F_8 source bottle. This will help put the pressure differential at around 10 psi;

5- Push LAB until no more C_3F_8 is seen coming from the fill line.

A.6. PICO-0.1 pressure system

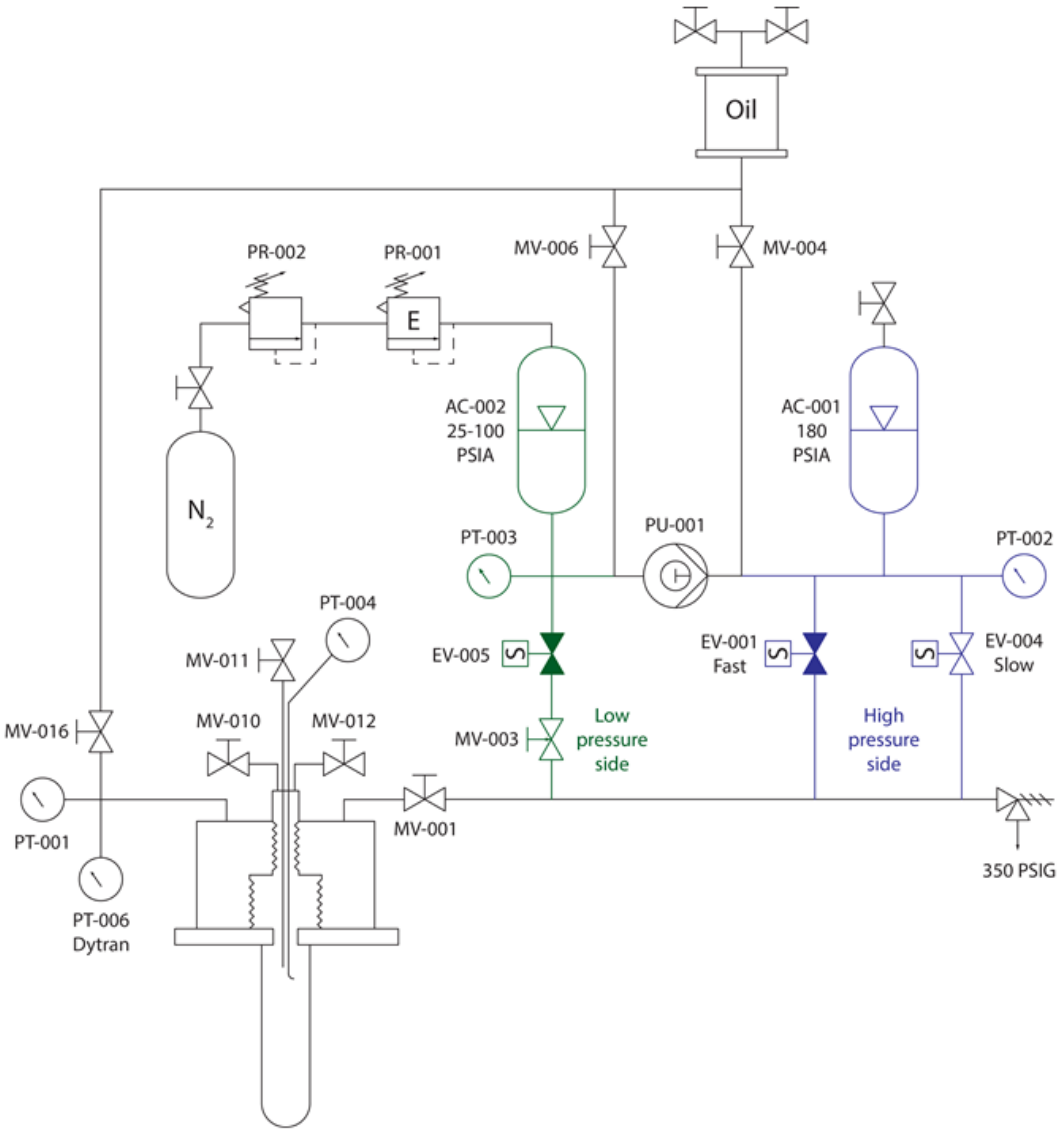

Figure A.1. Diagram of the pressure system of PICO-0.1